The Meteoritical Society

Meteoritics & Planetary Science 44, Nr 10, 1589–1609 (2009)
Abstract available online at http://meteoritics.org

A cometary aggregate interplanetary dust particle as an analog for comet Wild 2 grain chemistry preserved in silica-rich Stardust glass

Frans J. M. RIETMEIJER

Department of Earth and Planetary Sciences, MSC 03-2040, 1-University of New Mexico, Albuquerque, New Mexico 87131–0001, USA
Corresponding author. E-mail: fransjmr@unm.edu

(Received 19 December 2008; revision accepted 14 June 2009)

Abstract–Many of the nanometer-scale grains from comet 81P/Wild 2 did not survive hypervelocity capture. Instead, they melted and interacted with silica melt derived from the aerogel used by the Stardust mission. Their petrological properties were completely modified, but their bulk chemistry was preserved in the chemical signatures of mostly vesicular Si-rich glass with its typical Fe-Ni-S compound inclusions. Chondritic aggregate IDP L2011A9 that experienced atmospheric pre-entry thermal modification was selected as an analog to investigate these Wild 2 chemical signatures. The chemical, petrologic, and mineralogical properties of the individual constituents in this aggregate IDP are presented and used to match the chemical signatures of these Wild 2 grains. Mixing of comet material and pure silica, which is used in a diagram that recognizes this mixing behavior, is used to constrain the probable petrologic and minerals that caused the Wild 2 signatures. The Wild 2 nanometer-scale grain signatures in Si-rich glass allocations from three different deceleration tracks resembled mixtures of ultrafine-grained principal components and dense agglomerate-like material, Mg-rich silicates (<500 nm) and Fe,Ni-sulfides (<100 nm), and Si-rich amorphous material. Dust resembling the mixed matrix of common chondritic aggregate IDPs was present in Jupiter-family comet Wild 2.

INTRODUCTION

Comet 81P/Wild 2 (henceforward Wild 2) particles that produced bulbous deceleration tracks were "weakly constructed mixtures of nanometer scale grains, with occasional much larger (over 1 micrometer) ferromagnesian silicates, Fe-Ni sulfides, Fe-Ni metal, and accessory phases" (Zolensky et al. 2006). We do not know the sizes or size distributions of the nanometer-scale grains, if they were composite or single-grains, or small aggregates. That the very first comet dust particles ever to be collected were "weakly constructed mixtures" (Zolensky et al. 2006) evokes images of chondritic aggregate interplanetary dust particles (IDPs) rather than lithified clumps with meteorite-like structural properties. These IDPs are structurally and petrologically different from any materials present in the meteorite collections and therefore they are from parent bodies that are different from those that produced meteorites (Mackinnon and Rietmeijer 1987). These collected IDPs and cluster IDPs (Rietmeijer 1998a,b), are not weakly constructed mixtures as they survived deceleration in the Earth's atmosphere. When not part of an active meteor stream they spent 10^5–10^6 years spiraling towards the Sun which provides ample time for space weathering, e.g., polymerization of indigenous hydrocarbons, that will increase the initial material strength (Rietmeijer 1998a,b). In active meteor streams their orbital ages are generally short but not more than a few millennia (McNaught and Asher 1999; Lyytinen and van Flandern 2000; Jenniskens 2006). From the observed material strength and unusually low Na contents of meteors from the Geminid meteoroid stream, Borovička et al. (2005) hypothesized that the material strength was increased due to thermal desorption of sodium when nearing the Sun. In both cases these processes will affect the most volatile element abundances. They will probably not significantly modify the silicate and sulfide compositions found in aggregate IDPs and cluster IDPs (Rietmeijer 2000, 2005) but partial or complete amorphization by energetic solar particles as was documented in diopside and Mg-wollastonite (Rietmeijer 1999a) might have occurred.

There is a presumption that the most primitive solar system materials will have a chondritic bulk composition. The nanometer-scale comet Halley dust (Fomenkova et al. 1992) may not have been chondritic. Jessberger et al. (1988), and I quote, "may have missed a very important finding!" when they accepted the observed deviations of Si/Mg and Fe/Mg from their CI abundances to be within the uncertainty of the ion yields used. In addition, Leonid and Perseid meteors from

Halley-type comets 55P/Tempel-Tuttle and 109P/Swift-Tuttle, respectively, have >CI sodium and >Si abundances (Rietmeijer and Nuth 2000, Borovička 2005, 2006), and >CI sodium in comet Hale-Bopp (Rietmeijer 1999b). Volatile elements in excess of their CI abundances were reported in comet Wild 2 (Flynn et al. 2006). Do we have flawed expectations of the chemical, and perhaps also the petrologic and structural properties of comets, or could there be different types of comets? How are cometary chondritic aggregate IDPs (Bradley and Brownlee 1986) fit into the picture?

Reviewing the limited petrological database on IDPs, including cluster IDPs and their fragments, Rietmeijer (2002) found two types of chondritic IDPs, viz. aggregate IDPs with a considerable range of particle porosity and non-aggregate particles. My working model (Rietmeijer 1996a–c, 1998a, 2002) for comet dust provides for

1. Nanometer-scale grains, typically <500 nm, that include ultrafine-grained and coarse-grained principal components (PCs) with admixed nm-scale sulfides and silicates in aggregates that resemble the matrix of chondritic aggregate IDPs (see following discussion on PCs),
2. Micrometer-scale, ~1 to ~5 μm, Fe,Ni-sulfides, mostly (Mg,Fe,Ca)silicates and Si-rich amorphous grains (± Ca, Al, and Mg), and
3. Micrometer, ~10 to ~20 μm, silicate, sulfide and (Ca, Al, Ti)-refractory particles that can be monomineralic grains or compact poly-mineral agglomerates.

These minerals form a large fraction of the micrometer-scale minerals scattered along Stardust deceleration tracks and among the ~8 μm to ~15 micrometer terminal particles (Brownlee et al. 2006; Zolensky et al. 2006, 2008, Leroux et al. 2008a; Matrajt et al. 2008; Nakamura et al. 2008; Tomeoka et al. 2008). There are few surviving nanometer-scale Wild 2 grains, i.e., a few Mg-rich olivine, pyroxene and "FeS" grains in Si-rich glass (Leroux et al. 2008b), and a dense aggregate of nanometer-scale grains in the wake of a terminal particle (Matrajt et al. 2008). Evidence that nanometer-scale Wild 2 grains were abundant is still lacking.

The design of the under-dense, density graded (0.02 to 0.05 g/cc) Stardust aerogel allowed comet Wild 2 grains to survive in a size-dependent manner and favoring diffusion-less processes. A great many ~10 to 20 μm silica-rich glass clumps were found in the wall of bulbous deceleration tracks and along their stylus or styli. It seems plausible that a vast majority of nanometer-scale comet grains were flash-melted when they were forced into the wall of an expanding cavity at high temperatures (2000 up to ~5000 K?) where they encountered molten silica aerogel. Under these conditions intact survival of IDP-like matrix material was highly unlikely. First assessments of heating and cooling rates, and duration of the events, converge on 0.1 μs (1200 °C) to ~1 s (200 °C) for Fe-S diffusion in zoned sulfide nanograins (Rietmeijer 2008) with cooling rates between 2×10^7 and 10^8 K/s (Roskosz at al. 2008a; Leroux et al. 2008c) and with post-impact temperatures staying at ~2100 K for up to 0.1 μs based on MgO and SiO_2 diffusion between molten comet dust and silica melt (Roskosz et al. 2008b) that these authors consider to be characteristic for friable and fine-grained aggregates. For comparison, olivine, pyroxenes, and Fe-oxide nanometer grains in ultrafine-grained PCs formed in 5–10 s at cooling rates of 25–250 °C/s during atmospheric entry (Rietmeijer 1996a). In both cases melting, nucleation and grain growth could replace the original nm-scale minerals.

When nanometer Wild 2 dust resembled materials in the matrix of the chondritic aggregate IDPs, it is expected that almost all original minerals will be obliterated during hypervelocity impact capture. It is also expected that the bulk chemistry of the nanometer-scale Wild 2 grains be preserved in the Si-rich Stardust glass. While avoiding most of the omnipresent Fe-Ni-S inclusion, (Mg + Ca) versus Si (el%) correlations measured in silica-rich glass were consistent with serpentine-dehydroxylate, pyroxene, and smectite-dehydroxylate compositions of the constituents in the matrix of aggregate IDPs (Rietmeijer 2007). The comet's silicates (mostly Si, Mg, Al, Ca, and some amount of Fe) were as fully assimilated in the pure silica melt (Leroux et al. 2008b; Rietmeijer at al. 2008; Tomeoka et al. 2008). The numerous, typically <100 nm electron-opaque Fe-Ni-S inclusions (Leroux et al. 2008b; Rietmeijer at al. 2008; Tomeoka et al. 2008; Zolensky et al. 2008) were derived from Wild 2 sulfides. The low-Ni Fe-S and high-S Fe-S eutectic and deep metastable eutectic compositions of the inclusions suggest Si-rich melt temperatures >1200 °C (Rietmeijer 2008; Rietmeijer et al. 2008).

The Si-rich glass clumps appear to be porous agglomerates of smaller (quenched) melt droplets (see images in Nakamura et al. 2008; Rietmeijer et al. 2008). It is tempting to think that the extracted clumps are the "frozen" agglomerates by an instantaneous thermal transformation without chemical or physical mixing of structurally coherent, low-porosity nanometer scale agglomerates of smaller Wild 2 minerals and amorphous materials. It is hypothesized that aggregate IDPs consist of a limited number of specific constituents that are repeated in a hierarchical (fractal) manner as dust evolved and accreted into larger aggregates such as cluster IDPs from smaller chondritic aggregate IDPs and non-chondritic dusts (Rietmeijer and Nuth 2002, 2004).

This paper presents the chemical compositions and petrologic properties of the constituents in chondritic aggregate IDP L2011A9 for the purpose of comparing their chemical signatures with those left behind by Wild 2 grains in the Si-rich Stardust glass clumps. It should be possible to constrain nanometer-scale Wild 2 grain properties in terms of aggregate IDP petrology. This IDP was selected because:

1. It is a common particle that contains all constituents typically present in aggregate IDPs.
2. It experienced post-aggregation modification whereby partial fusion of the PCs caused local textural collapse

and strengthening of the matrix while in other areas the boundaries between PCs became very fuzzy accompanied by new growth of nanometer sulfides. Its material strength properties might be closer to Wild 2 grains compared to a highly porous aggregate.

3. Sulfur is present at its CI level and yet it has fine-grained, polycrystalline Fe-oxide segments along its periphery to suggest that it experienced only very mild atmospheric entry flash-heating using the criteria of Flynn (1994a).
4. Its mild thermal modification probably took place when still resident in a parent body that if it was a Jupiter-family (J-F) comet may have experienced transient collisional heating, including catastrophic disruption (Brown et al. 2007). The cratered surface seen "up close" on J-F comets 19P/Borrelly (Soderblom et al. 2002), Tempel 1 (A'Hearn et al. 2005), and Wild 2 (Brownlee et al. 2004) suggest they experienced dynamic environments. It is unlikely though that most of these craters are impact craters.

EVOLVED-CONDENSATE OR IRRADIATION-INDUCED GRAINS, OR BOTH

The matrix of aggregate IDPs is dominated by ~90 nm to ~500 nm in diameter (sub)spherical ferromagnesiosilica grains. The first, and most common, type of these grains have an amorphous matrix that contains nanometer-size sulfides and metals; second, less common grain type contains a Mg-rich pyroxene, a Mg-rich olivine and an amorphous silica-rich material ± variable, minor amounts of Al, Ca, Mg, and Fe. What to call the second grains is less obvious. Both types have entered the literature under a bewildering array of names (see review by Rietmeijer 1998a), that include coarse-grained and ultrafine-grained Principal Components (Rietmeijer 1996b, 1996c); tar balls, GEMS, i.e., glass with embedded metals and sulfides, and unequilibrated units (Bradley 1988, 1994a, 1994b).

Kinetically controlled vapor phase condensation experiments (Rietmeijer et al. 1999a) showed that amorphous, high-Mg ferromagnesiosilica grains could form by agglomeration and fusing of amorphous MgSiO and FeSiO condensates (Rietmeijer 2002). The grain compositions are specific, predictable, and uniquely controlled by non-equilibrium vapor phase condensation. Their Mg/(Mg + Fe) (at) ratios are >0.65; Mg/Si ratios (at) range from almost pure silica to 1.5. These less common grains had a history of condensate evolution prior to IDP accretion. They are referred to as coarse-grained principal components (Rietmeijer 1998a, 2002).

The petrographic texture of all of the first and most common type of grains in the matrix of aggregate IDPs adequately fits the GEMS texture. However, the name GEMS was initially given to objects that had formed by preaccretional irradiation (Bradley 1994a). At present the GEMS label is inexorably linked to this very specific origin but it was only a hypothesis (Bradley and Ishii 2008). The hypothesis was tested and found lacking (Martin 1995) and it is still challenged as being the amorphous silicate in the interstellar medium (Min et al. 2007). There is still no experimental verification that irradiation-induced amorphization of enstatite and pyrrhotite (Bradley 1994a) will lead to the formation of an object with an amorphous ferromagnesiosilica matrix with tiny inclusion of sulfides and metal. There is no evidence that irradiation-induced amorphization (Bradley 1994a) is the only process that could form such objects. Flynn (1994b) already suggested the alternative origin that GEMS could be solar nebula condensates.

Non-equilibrium vapor phase condensation also cannot produce amorphous grains with petrological and chemical properties attributed to GEMS (Rietmeijer 2002). Still, non-equilibrium condensate evolution leads to amorphous, coarse-grained PC that, when reacting with Fe-metal or FeO condensates, or sulfidized Fe-metal grains, or all, would yield grains with the compositions of original GEMS (Bradley 1994a) as well as compositions that are currently attributed to GEMS with widely variable Mg/Si ratios (el) and Mg/(Mg + Fe) (el) ratios ranging from ~0.2 to ~0.65 (Keller and Messenger 2004), as well as the deep metastable eutectic ferrosilica composition of a large sphere in IDP L2011A9 described in this paper.

Ufg PCs are petrographically describable as GEMS and whether their matrix is glass or an even more disordered amorphous material seems to be a moot point at this time. The chemical properties of ufg PC match the narrowly constrained original GEMS composition (Bradley 1994a) and include the broader range currently accepted (Keller and Messenger 2004). The difference between GEMS and ufg PCs refers to their hypothesized mode of formation as preaccretionally induced-amorphization (Bradley and Ishii 2008) or chemically evolved non-equilibrium condensates (Rietmeijer 2002), respectively. Ufg PCs cannot contain relics of partially amorphized silicate or sulfide minerals but such grains were found in GEMS. The origin of a (sub)spherical grain with a GEMS or an ufg PC composition but lacking a relic grain or a vesicular texture that is indicative for irradiation-induced amorphization remains uncertain. In such cases I prefer the descriptive designation "ugf PCs," which will be used in this paper. Finally, the GEMS-like objects in Stardust aerogel could be either "real" GEMS or ufg PCs that escaped mixing with silica melt (Leroux et al. 2008b; Tomeoka et al. 2008), or they might represent an entirely new mode of formation that is unique to the Stardust capture process.

EXPERIMENTAL PROCEDURES

Particle L2011A9 was embedded in Spurrs epoxy at the NASA Johnson Space Center Curatorial Facility for serial sectioning using a Reichert-Jung Ultramicrotome E using a diamond knife speed between 0.5 and 0.8 mm s^{-1} at the

Electron Microbeam Analysis Facility (UNM). The 80–100 nm thin sections were placed on a holey carbon thin-film supported by a standard 200 mesh Cu grid and housed in a Gatan low-background, double-tilt specimen holder. The sections were analyzed using a JEOL 2000FX analytical and transmission electron microscope (ATEM) that was operating at 200 keV and was equipped with a Tracor-Northern TN-5500 energy dispersive spectrometer (EDS) for in situ analysis of elements >11 atomic number using a 15 nm probe size.

The Stardust allocations C2054,0,35,44,6, C2004,1,44,4,3 (Rietmeijer 2007), and C2092,2,80,47,6 consisted of several serial sections on a 10 nm amorphous carbon film supported on a Cu TEM grid at NASA Johnson Space Center Stardust Curatorial Facility. Analyses were performed using a JEOL 2010 high-resolution transmission electron microscope (HRTEM) that operated at a 200 keV accelerating voltage and was equipped with an ultrathin-window energy dispersive X-ray detector for quantitative chemical analyses (Zolensky et al. 2006, supplemental data). A focused analytical probe size (5, 10, or 15 nm) was selected to be smaller than the object of interest wherever possible but maintaining an optimum combination of the electron beam probe size and EDS acquisition time nut preserving statistically relevant signal-to-noise ratios. The compositions of the numerous electron-opaque Fe-Ni-S inclusions in the Si-rich Stardust glass contains (Zolensky et al. 2006) smaller than ~35 nm will be difficult to determine accurately in 70 nm-thin TEM sections unless present in favorable textural conditions. The very smallest inclusions might be missed and could inadvertently cause very low Fe, Ni, and S abundances to be attributed to the glass composition. Quantitative chemical data were obtained using the Cliff-Lorimer (1975) thin-film procedure for experimentally determined *k*-factors used at UNM. For EDS data reduction of L2011A9 the operator selected a background that was compared to a standard as well as random IDP spectra for check for internal consistency when accumulating a database. The error bars on minor elements was ~10% relative. For the conditions of Stardust samples see Zolensky et al. (2006, supplemental data) but the data reduction program indicates when an element is present near the two-sigma level for most of the element abundances in the flight aerogel, which was the accepted limit. Element and oxide abundances were reduced for stoichiometric compositions. Oxygen is then calculated by difference; no oxygen data are presented in this paper. Sulfides are reported in atomic abundances. Phase identification was made by a combination of selected area electron diffraction (SAED), HRTEM imaging and chemical data. The location of each analysis was recorded on TEM images for assessment of any spurious artifacts, e.g., multiple grains along the electron beam path or overlapping grains, which went unnoticed during the data acquisition. Grain size was measured with a <10% relative error. The reported grain sizes and compositions are normal distributions at a 95% significance level based on the ratio range/standard deviation (1σ) as a function of population size (N).

OBSERVATIONS

Chondritic Aggregate IDP L2011A9 Properties

Aggregate Constituents

At its largest scale this ~18 μm × ~10 μm IDP is a high porous aggregate (Fig. 1a) of several units. Some of these units are agglomerates of various smaller units that can for compact masses or can be somewhat porous aggregates (Fig. 1b) wherein the units had fused, often with fuzzy boundaries. In such agglomerates the units in variable relative proportions. Locally the original units were modified beyond recognition. The textural units are

1. Mostly densely packed ufg PCs with scattered nm-scale Fe,Ni-sulfides.
2. Massive, amorphous Si-rich grains with variable amounts of Mg, Fe, Al and Ca that include a few interspersed Fe-sulfides, including a compact, 2 μm × ~1 μm, Si-rich unit called Big Guy (Rietmeijer 1994a, 2002).
3. Patches of mixtures of sulfide grains, cg PCs, amorphous Si-rich material, rare amorphous aluminosilica grains with embedded silicates, and compact polycrystalline clusters of silicates and sulfides in an amorphous matrix (Fig. 2).
4. Small agglomerates ranging from mostly silicates with one or a few nm-size sulfides to (rare) dense polycrystalline sulfide clusters with associated silicates.
5. An electron-opaque sphere.
6. A single 1 μm Fe,Ni-sulfide.

The textures support densification of a porous aggregate particle and local re-crystallization. The compositional scatter in this anhydrous aggregate IDP is dominated by cg PCs and high-Fe ufg PCs (Fig. 3) with Mg/(Mg + Fe) (el) < 0.65 (Rietmeijer 1996b, 1996c, 1998a, 2002).

Dense Agglomerate Bulk Composition

The Si- and CI-normalized (Anders and Grevesse 1989) abundances of the calculated bulk composition (Table 1) show (1) slightly below average CI abundances for most elements but a CI sulfur abundance and (2) an extensive range for all elements with Mg and Al systematically below their CI abundance (Fig. 4). The Fe/Ni ratio, 22 ± 7.8 (range: 9–41), is a perfect match with the cosmic Fe/Ni ratio. About 20% of the agglomerates are Cr-free. When present it ranges from 0.1 to 0.6 Cr_2O_3 wt% ($\mu \pm \sigma = 0.3 \pm 0.2$). About 60% of agglomerates contain Mn, MnO = 0.05–0.35 wt% ($\mu = 0.15 \pm 0.1$). The remainder is both Mn- and Cr-free. A third of agglomerates are Ca- and Al-free. When present CaO ranges from 0.05 to 2.35 wt% ($\mu = 1.2 \pm 0.75$). About 80% of agglomerates contain Al ranging from 0.4 to 9.6 Al_2O_3 wt% (μ

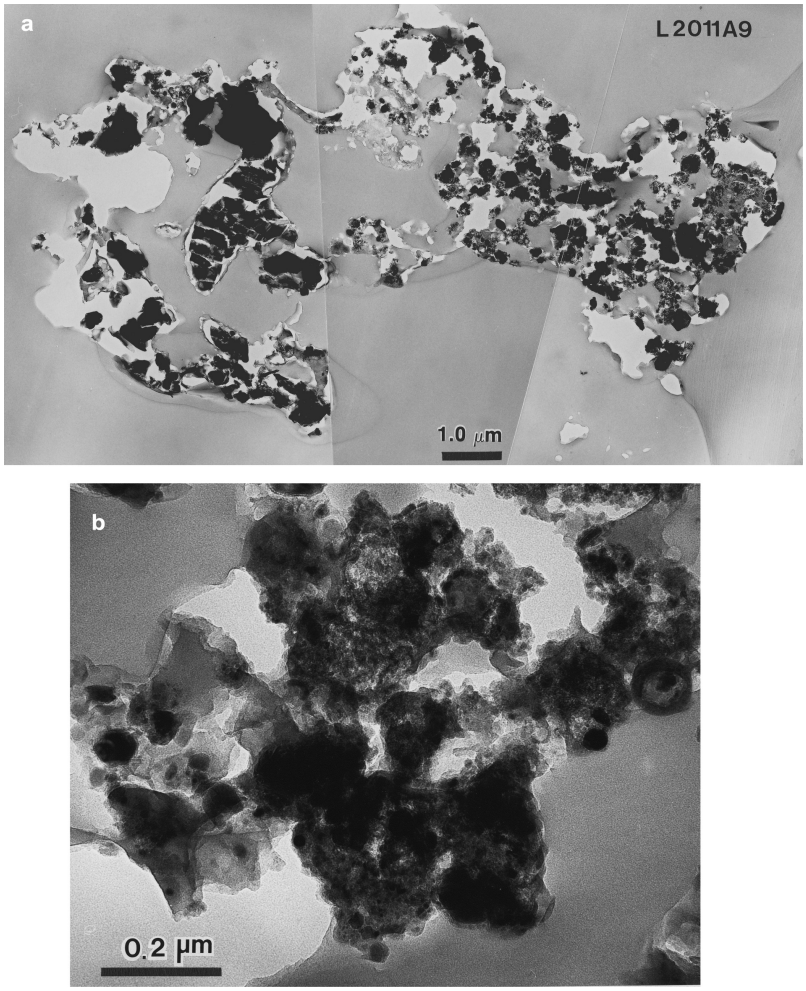

Fig. 1. a) A transmission electron microscope image of one section through porous chondritic aggregate IDP L2011A9 showing the Big Guy unit (bean-shaped grain on the left-hand side) and the only large sulfide grain in this IDP (opaque equant grain attached to Gig Guy). The massive-looking part to the lower left is dominated by are coarse-grained PCs. The embedding epoxy shows as the gray background; white areas indicate sample loss that is a common experimental artifact for ultramicrotome IDP sections. b) A detail showing a concentration of ultrafine-grained PCs, some of which were fused together.

= 1.7 ± 2.1; the modal value = 1.2 Al_2O_3 wt%). The highest alumina contents are in amorphous Big Guy (see below).

Ultrafine-Grained Principal Components

Dimensions and Grain Sizes

The smallest ufg PC is 30 nm in diameter; the largest is 360 nm across. Their mean diameter is 145 ± 65 nm. About 70% of ufg PCs are rounded often with an irregular surface (Fig. 5). The aspect ratios, i.e., ratio of the smallest to the largest dimensions, range from 0.45 to 0.9 ($\mu = 0.8 \pm 0.1$) for rounded to (rare) elongated ellipsoidal ufg PCs. For reference, a peanut-shaped unit of two partially fused units has a 0.5 aspect ratio. Their lognormal size distribution shows they grew by agglomeration and fusion.

The Fe,Ni-sulfide, Fe-oxide and Mg,Fe-silicate grains range from 0.7 to 75 nm with an average 2.6 nm size, which is common for ufg PCs (Rietmeijer 1994b; wherein the table refers incorrectly to U2011A9 instead of L2011A9). About 85% are rounded or equidimensional euhedral mineral grains; the remainder have aspect ratios between 0.4 and 0.9 ($\mu = 0.7 \pm 0.1$). The grains size distribution is intermediate between a lognormal and an exponential distribution which is consistent with second-order Ostwald ripening. It reflects different growth behaviors for silicates and sulfides in ufg PCs.

Compositions

The bulk compositions show a division in low-MgO ufg PCs and five high-MgO ufg PCs (Table 2). The average Si- and CI normalized abundances are close to the CI abundances with the largest deviations for S and Ca. All elements show a considerable range of abundances (Fig. 6). The sulfur abundances (Fig. 6) indicate a complete range from FeS to Fe-metal grains. The ufg PCs are Mn- and Cr-free. About 15% of low-Mg PCs contain potassium, 0.4 ± 0.4 el% K (range: 0.02–1.2) that appears to be indigenous to these particular PCs.

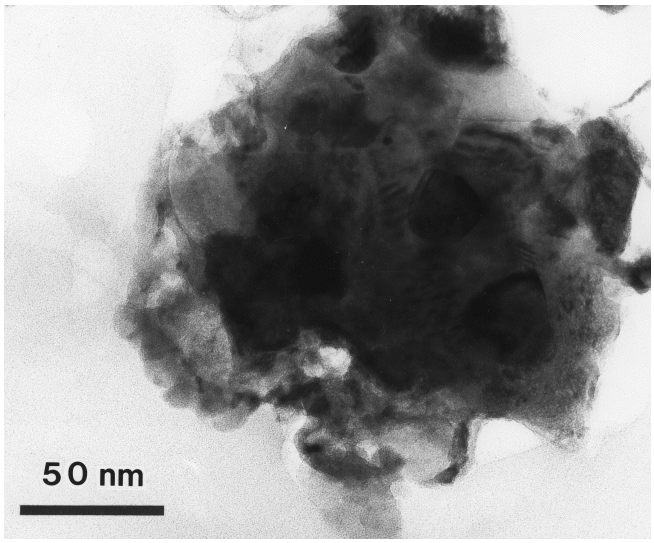

Fig. 2. A transmission electron microscope image of a section through a compact polycrystalline cluster of silicates and sulfides in an amorphous matrix that is a thermally modified, coarse-grained PC in chondritic aggregate IDP L2011A9.

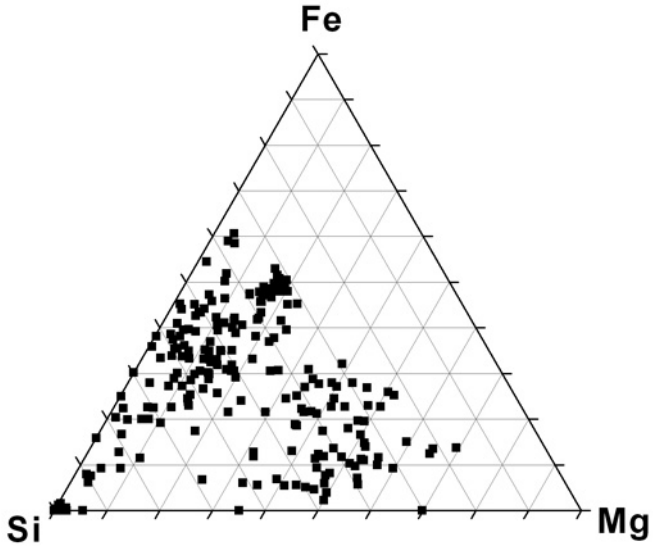

Fig. 3. The ternary diagram Mg-Fe-Si (el%) showing the compositional variability caused by the diversity amorphous Si-rich materials and silicates in aggregate IDP L2011A9. The compositions of the large Fe,Ni-sulfide grains are not shown.

Alumina has a weak affinity for Si-rich, low-MgO ufg PC (~6 wt% Al_2O_3), gradually decreasing to ~1 wt% Al_2O_3 when Mg/(Mg + Si) is ~0.5. Three ufg PCs are alumina rich with 8–12 wt% Al_2O_3). In general the sulfur contents of ufg PC vary considerably as a function of the Mg/(Mg + Fe) element ratio (Fig. 7). This scatter is much less in ufg PCs with fuzzy outlines that are embedded within dense agglomerates. Their textures suggest they formed during a post-accretion heating event. Fe-rich ufg PCs have higher sulfur contents than Mg-rich ufg PCs (Figs. 3 and 7). The high-S, Fe-rich ufg PCs require

Table 1. Calculated bulk composition (wt%) of dense-packed agglomerates in aggregate IDP L2011A9; mean ± one standard deviation ($\mu \pm \sigma$). This composition is considered to represent the bulk composition, although it does not include the amorphous Si-rich Big Guy unit.

	$\mu \pm \sigma$
SiO_2	47.0 ± 9.2
MgO	16.8 ± 6.3
Al_2O_3	1.3 ± 2.1
CaO	0.9 ± 0.9
Cr_2O_3	0.2 ± 0.15
MnO	0.09 ± 0.12
FeO	24.4 ± 8.0
NiO	1.1 ± 0.7
S	7.3 ± 3.1

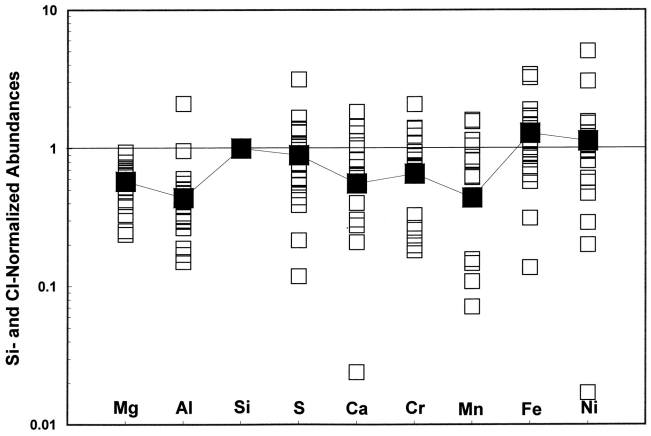

Fig. 4. Si- and CI-normalized element abundances (Table 1) for dense agglomerates in aggregate IDP L2011A9 (open squares) and the calculated average abundances (solid squares).

mixing a "silicate" source such as cg PCs in this IDP and a "Fe-containing" source (see below). Textural evidence suggests that some cg PCs reacted with Fe-sulfides in dense agglomerates. In fact, an Fe,Ni-sulfide is commonly found in contact with a cg PC (Rietmeijer et al. 1999a), which makes coincidence for this association seem unlikely. A few low-MgO and most high-MgO ufg PCs have a smooth round outline with grains showing evidence of coarsening. Their seriate textures indicate thermal modification. They show some resemblance to porphyritic glass in other IDPs (Joswiak and Brownlee 1998, 2006).

Coarse-Grained Principal Components

Dimensions and Grain Sizes

They range from 135 nm for a perfectly round cg PC to 1,400 nm in diameter. The mean diameter is 500 ± 260 nm. The modal diameter of 395 nm causes a skewed (S = 0.4) normal distribution indicating that large cg PCs, e.g., the largest, highly elongated cg PC of 1,850 nm × 690 nm, formed by fusion of smaller ones. Amorphous and mineral grains in cg PCs range from 8 nm to 385 nm; μ = 103 ± 82.5 nm;

Table 2. Bulk compositions (el%) for low-Mg and high-Mg ultrafine-grained PCs in aggregate IDP L2011A9; *N*: number of PCs. The modal values are for non-Gaussian normal distributions. The high-Mg PCs include three S-free PCs; in the others S = 0.7 and 1.4 wt%; four PCs are Ni-free, in the other Ni = 0.5 wt%.

	Mg	Al	Si	S	Ca	Fe	Ni
			Low-Mg ultrafine-grained PCs [N = 47]				
Mean	6.9	1.5	21.5	4.8	0.5	19.4	1.3
Std. deviation	4.6	1.4	5.2	3.7	0.3	6.8	0.9
Range	0–19	0–6.5	12–37	0–15	0.02–1.5	1.5–35	0–5
Mode	3.0	–	–	0.9	–	–	–
			High-Mg ultrafine-grained PCs [N = 5]				
Mean	23.2	0.7	23.2	–	0	7.8	–
Std deviation	2.1	0.2	2.1	–	–	4.1	–
Range	20–25	0.5–1	20–25	–	–	1–12	–

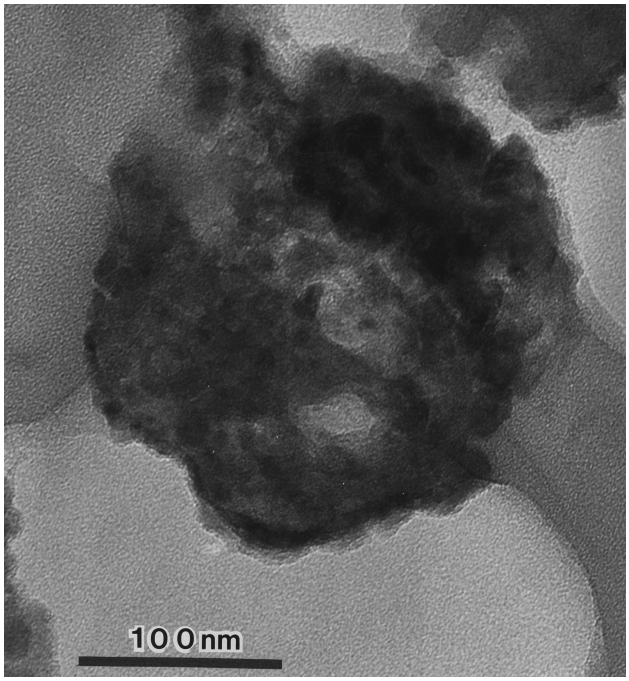

Fig. 5. A transmission electron microscope image of an ultrafine-grained principal component grain in chondritic aggregate IDP L2011A9.

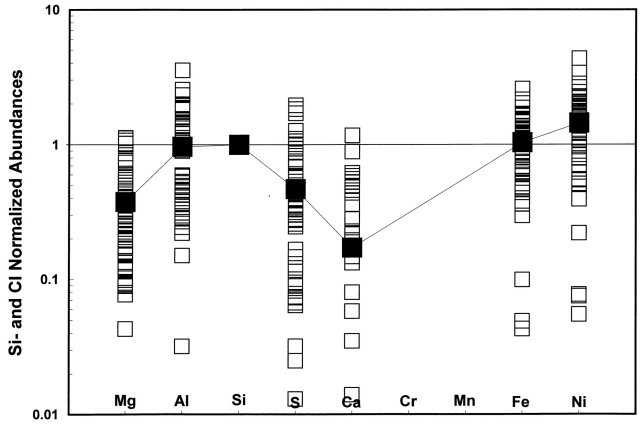

Fig. 6. Si- and CI-normalized element abundances of all ufg PC compositions (Table 2) in aggregate IDP L2011A9 (open squares). The average abundances (solid squares) were calculated including zero abundance. The normalized bulk Ca abundance for all CaO-containing ufg PCs is 0.38; the value (0.17) shown includes Ca-free ufg PCs. About 50% of low-Mg PCs is Ca-free. Such differences for the Al, S and Ni abundances would be much less dramatic.

only 30% is smaller than the modal size (68 nm). These grain sizes show a transition from a lognormal to an exponential distribution, indicating either loss of the smallest grains due to grain growth or a new population of small grains. The aspect ratios of these grains range from 0.2 to 1, with 95% having aspect ratios between 0.5 and 1; ~50% are equant but not necessarily rounded grains. The lath-shaped grains with the lowest aspect ratios are among the smallest grains observed.

Chemical Compositions

Amorphous Materials

A typical cg PC consists of an olivine, a pyroxene and an amorphous Si-rich grain (restite) wherein the silicates have identical Mg/ (Mg + Fe) ratios (Rietmeijer 1998a; Rietmeijer et al. 1999a). The amorphous and silicate grains are similar in size and occur in about equal proportions. Similar properties are found in the equilibrated units in other aggregate IDPs (Bradley 1988, 1994b). The largest cg PCs are amorphous, either pure silica or Si-rich restite grains (Rietmeijer 1998a, 2002). Some of these large amorphous grains have a few small, round sulfide inclusions or lath-shaped sulfide grains that resemble relict sulfide grains in quenched silicate glass associated with large sulfide IDPs (Rietmeijer 2004).

The full compositional range for each element is shown in Fig. 8 along with the calculated average, Si and CI-normalized element abundances (Table 3). The normalized Al-abundances (Table 3) define two normal distributions: (1) 0.44 ± 0.26 (0.015–0.98; N = 28), and (2) 3.20 ± 1.60 (0.29–7.48; N = 28 that is primarily caused by the cg PC Big Guy (Fig. 9a). It also has the highest Ca contents (Fig. 9b). Ca and Al co-occur in a third of the amorphous materials but they are entirely uncorrelated. The Mg and Si (el%) abundances show a weak anti-correlation in the amorphous grains

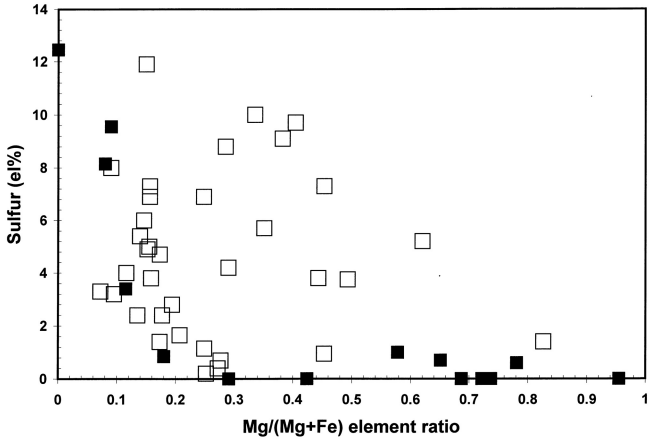

Fig. 7. The sulfur (el%) content versus the Mg/(Mg+Fe) (element) ratio for the most common ufg PCs in aggregate IDP L2011A9 (open squares) and in situ formed ufg PCs (solid squares).

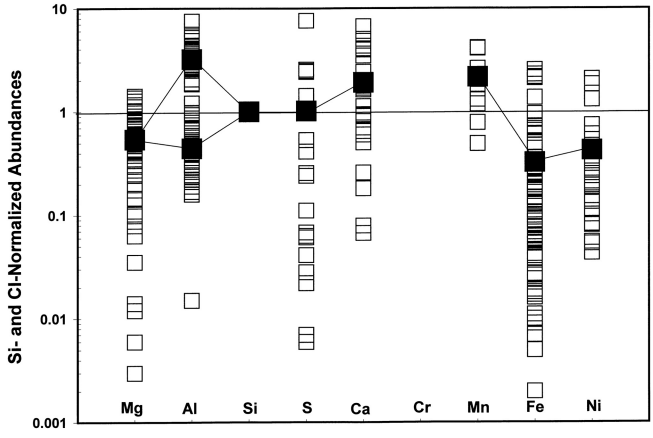

Fig. 8. The range of Si- and CI normalized element abundances for the amorphous grains inside coarse-grained PCs, cg PC Big Guy (see below), amorphous restite with and without sulfide inclusions, and the bulk compositions of the four smallest cg PC in aggregate IDP L2011A9 (open squares). The normalized calculated average elemental abundances (Table 3) including both Al populations are also shown (solid squares).

associated with the silicates in cg IDPs (Fig. 10). The widely variable Mg contents at almost constant Si support that Big Guy is an agglomerate of fused amorphous grains.

The Al-rich silicate "non-GEMS interstitial silicate glass" in other chondritic aggregate IDPs (Joswiak and Brownlee 2006) shows a chemical resemblance to silica-rich amorphous restite grain that incorporated Al and Ca that could not go into co-occurring olivine and orthopyroxene in the cg PCs. The common association of these silicates and amorphous grains suggests decomposition and partial crystallization of amorphous precursors (Rietmeijer 1999c, 2002). One amorphous grain has a stoichiometric enstatite composition.

Sulfides

Ni-free and low-Ni (2 at%) Fe-sulfides in the amorphous grains are generally rounded. They range from 35 nm to rare ellipsoidal grains up to 60 nm × 45 nm, which is well below the modal size range for isolated sulfides scattered throughout this IDP. The sulfur contents scatter around FeS, 48.9 ± 3.6 at% S (Fig. 11). Further, there is a small amorphous, high-S compound, a high-Ni sulfide, $Fe_{52.6}$ $Ni_{4.0}$ $S_{43.4}$ grain (Fig. 11) and a few small kamacite, $Fe_{0\text{-}9}Ni_{0.1}$ grains.

Silicates

Silicates in cg PCs are typically (75%) olivine plus (1) Ca-free pyroxene, Mg/(Mg + Fe) (*mg*) = 0.74, low-Ca pyroxene ($En_{70}Fs_{25}Wo_5$) or Ca-rich pyroxene (Table 4). One third of the pyroxenes is Ca-free pyroxene; Ca-rich pyroxene is present in ~25% of cg PCs. Olivine ranges from (rare) pure forsterite, *mg* = 0.93 to olivine, *mg* = 0.78 that may contain minor amounts of Al, Mn and Ni (Table 4). The similar *mg*-ratios (Fig. 12) support co-genetic origins for the silicates in a closed system. Manganese is present in 75% of Ca-rich pyroxene. Diopside, $En_{50}Fs_2Wo_{48}$, has the highest Ca content (14.2 el%). The Wo-contents appear to be bimodal (Fig. 13) but they are inconsistent with co-existing equilibrium phases (cf. Lindsley and Andersen 1983). The silicates in cg PCs are mostly between ~100 nm and ~500 nm (Fig. 14).

The normalized element distributions for the silicates show a considerable range for each element (Fig. 15). The calculated average silicate compositions show that the highest Ca contents are entirely due to Ca-rich pyroxene. Sulfur and commensurate fractions of Fe and Ni are most likely contaminants from FeS grains. Still, some amount of Ni is indigenous to olivine and Ca-free and low-Ca pyroxenes. The silicates in the cg PC show a moderate linear anti-correlation (r^2 = 0.79) between Mg and Si el% (Fig. 16). These similar trends support co-genetic relationships between these silicates and amorphous materialsf in cg PCs.

Isolated Fe- and Fe,Ni-Sulfides

Sulfides with compositions that cluster around stoichiometric FeS (Fig. 17) are dispersed throughout the dense agglomerates. The Ni-free and low-Ni (<2 at% Ni) sulfides form two groups based on sulfur content (Table 5). Sulfides S >50 at% are overwhelmingly angular grains with a mottled or striated oxidation texture and vesicles caused by atmospheric entry flash heating (Rietmeijer 2004). Sulfides S < 50 at% generally have no flash heating textures. Sulfur hotspots (Fig. 17) are amorphous Fe-S compounds. The low-sulfur Fe-S compositions are for a single subhedral Ni-free grain (690 nm × 540 nm; S = 20 at%) and a grain with S = 30 at% (Table 5).

Ni-free and low-Ni sulfides range from 38.5 nm in diameter for equant grains to mostly angular and (rare) euhedral, grains up to 930 nm × 705 nm. Most grains are between 125 nm ×

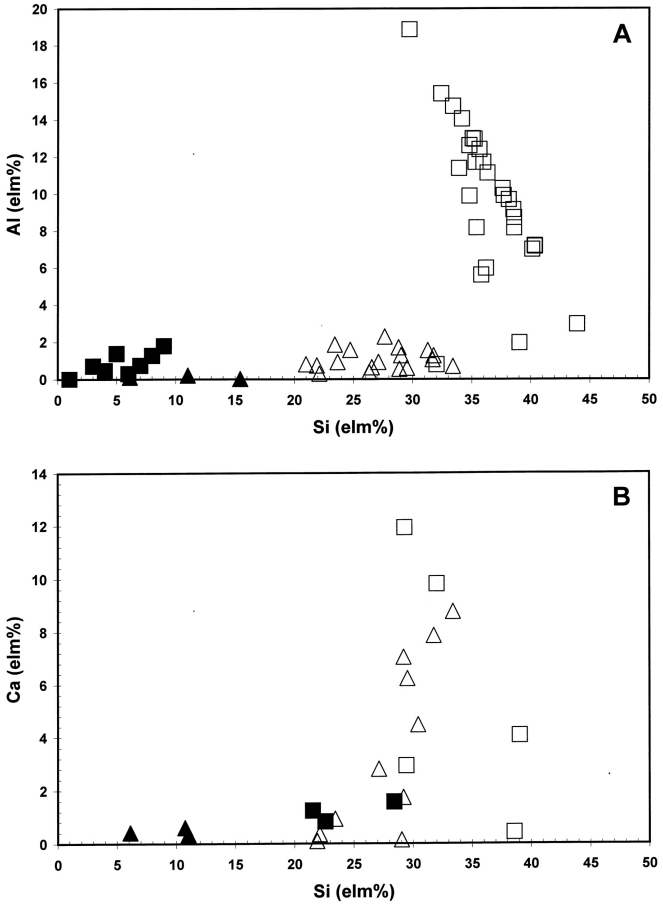

Fig. 9. a) Al versus Si (el%) and b) Ca versus Si (el%) in amorphous materials in aggregate IDP L2011A9 that include Big Guy (open squares), amorphous grains with (solid squares) or without (open triangles) sulfide inclusions, and the four smallest cf PC bulk compositions (solid triangles; two compositions overlap).

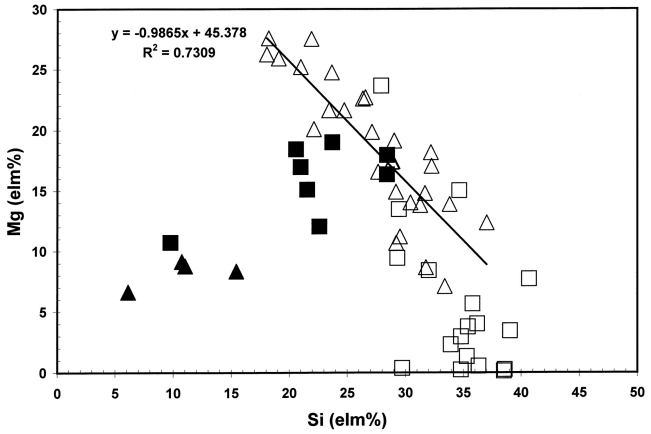

Fig. 10. Si versus Mg (el%) of the constituents among the amorphous cg PC materials in aggregate IDP L2011A9 (same symbols as in Fig. 9).

90 nm (angular grain; low-Ni, group 2) and 70 nm × 95 nm for a vesicular euhedral grain (low-Ni, group 1). In order to compare the size of non-spherical or equant grains, it is useful to calculate the root-mean-square (*rms*) size, i.e., rms = $\{a^2 + b^2\}^{1/2}$, where *a* and *b* are two orthogonal dimensions across a grain. The *rms* size for the angular grains range from ~40 nm to ~1200 nm, with a modal size range between 180 nm and 200 nm. There is no correlation between *rms* size and the sulfur content.

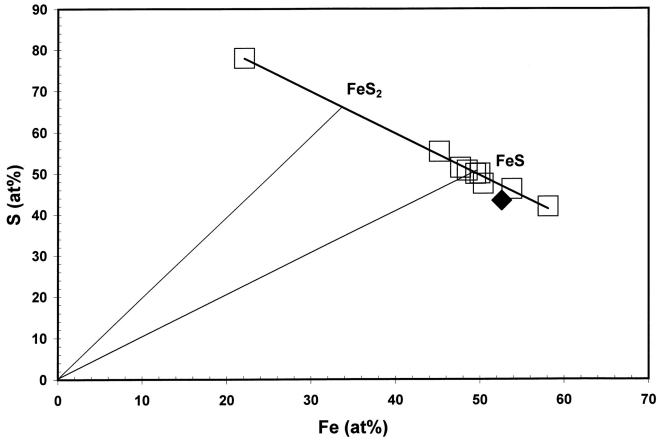

Fig. 11. Fe versus S (at%) for Ni-free and low-Ni sulfides (open squares) embedded in amorphous materials of cg PCs in aggregate IDP L2011A9, an amorphous high-S FeS compound, and a high-Ni sulfide grain (solid diamond).

Rare subhedral and angular grains between 140 nm × 80 nm and 540 nm × 130 nm are Ni-rich sulfides. Compositionally they resemble the high-Ni sulfide core of sulfide IDP L2005E40 (Rietmeijer 2004) and "polycrystalline mafic sulfide grains," including a grain with a pentlandite-like composition but a cubic spinel-like structure, in IDP U2015*B2 (Dai and Bradley 2001).

MISCELLANEOUS

A round grain (Ø = 865 nm) with SiO_2 = 75 wt% and FeO = 25 wt% that is compositionally reminiscent of an amorphous compound with a deep metastable eutectic ferrosilica composition (Rietmeijer et al. 1999a,b, 2006). Its composition and shape suggest a quenched liquid origin.

An isolated amorphous patch (~400 nm × ~350 nm) has a porous, granular core and a partial rim of dense-packed ring structures. The core composition, MgO = 35% wt%, FeO = 58 wt% and SiO_2 = 7 wt%, matches low-SiO_2 ferromagnesiosilica compounds with deep metastable eutectic compositions (Rietmeijer et al. 1999a, 2002). It is probably magnesioferrite with trace amounts of Al and S, similar to magnesioferrite patches in chondritic aggregate IDP L2011A3 (Rietmeijer 1996d). In a pulse-heating experiment of pieces of the Tagish Lake meteorite magnesiowüstite formed at the expense of Fe-Mg carbonate (Nozaki et al. 2001). Recognizing the different redox conditions in this experiment and those preserved in the IDP, it is at least possible that Fe-Mg carbonate may have been present in this IDP prior to thermal modification in the parent body.

Table 3. Si- and CI-normalized element abundances for the amorphous materials in aggregate IDP L2011A9 (*N*: the number of analyses). All elements have normal distributions.

	Mg	Al	S	Ca	Mn	Fe	Ni
μ ± σ	0.54 ± 0.36	1.84 ± 1.81	1.02 ± 1.83	1.90 ± 1.85	2.15 ± 1.38	0.325 ± 0.56	0.43 ± 0.55
Range	0.01–1.4	0.02–7.8	0.01–7.6	0.7–6.7	0.49–4.1	0.01–2.5	0.04–2.1
N	58	56	19	22	26	67	24

Table 4. Si- and CI-normalized element abundances of silicates in coarse-grained PCs of aggregate IDP L2011A9. The elements have normal distributions (μ ± σ; *N*: number of measurements.

Mg	Al	Ca	Mn	Fe	Ni	
			Olivine			
μ ± σ	1.48	–	–	–	0.13	–
Range	–	–	–	–		–
N	3	–	–	–	3	–
μ ± σ	1.33 ± 0.13	0.30	–	1.5	0.54 ± 0.08	0.15
Range	1.1–1.6	–	–	–	0.4–0.6	–
N	15	3	–	3	15	3
			Ca-free and low-Ca pyroxenes			
μ ± σ	0.59 ± 0.06	0.45 ± 0.41	0.90 ± 1.14	1.63 ± 1.0	0.25 ± 0.12	0.62 ± 1.3
Range	0.5–0.70	0.03–1.30	0–1.15	0.33–3.50	0.01–0.43	0.04–3.56
N	26	15	19	18	26	19
			Ca-rich pyroxenes			
μ ± σ	0.31 ± 0.07	Trace	4.97 ± 2.53	1.25 ± 1.07	0.14 ± 0.09	Trace
Range	0.24–0.38	–	0.96–7.80	0.44–3.36	0.02–0.24	–
N	8	2	8	6	8	1

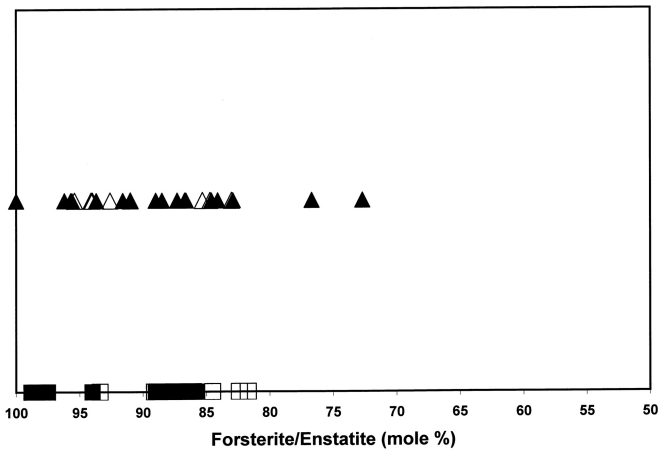

Fig. 12. Mole% forsterite for olivine (squares) and enstatite (mole%) for low-Ca (0 < Wo < 2 mole%) pyroxenes (triangles) in coarse-grained PCs (solid symbols), and isolated silicates (open symbols) in aggregate IDP L2011A9.

Comparing Wild 2 Signatures in Si-rich Glass and L2011A9

Probable Constituents of Nanometer-Scale Wild 2 Grains

Chondritic aggregate IDP L2011A9 was thermally modified prior to entering the Earth's atmosphere albeit not severe enough to entirely destroy the properties of its constituents because of its CI sulfur content but enough to cause partial loss of aggregate porosity when forming dense agglomerates. Pyrometamorphism of pyrrhotite during atmospheric entry heating will shift its composition towards pyrite with co-precipitating Fe-oxides but with continued heating sulfur will precipitate as pure sulfur (Rietmeijer 2004). The low-Ni Fe-S compound compositions in Stardust allocation C2054,0,35,24,1 show a different pattern of low-Ni Fe-S compounds S < 50 (at) and sulfur hot spots of amorphous low-Ni Fe-S compounds (Leroux et al. 2008b) that point towards reducing conditions when Wild 2 grains interacted with silica melt. A similar co-occurrence of sulfur hot spots and low-S Fe-S compounds in IDP L2011A9 (Figs.11 and 17) suggests that this particle experienced thermal modification under reducing conditions before it entered the Earth's atmosphere. The compositions from this parent body modification survived the relatively mild thermal conditions of IDP flash heating compared to the thermal conditions during capture of Wild 2 grains, whereby according to Leroux et al. (2009) indigenous comet sulfides destabilized and sulfur was readily volatilized to S_2.

Other textural and mineralogical evidence for thermal modification includes (1) seriate textures of some ufg PCs, (2) sulfur laths in amorphous grains, (3) secondary grain growth in cg PCs, (4) the ferrosilica sphere with a deep metastable eutectic composition, and (5) unequilibrated ufg PC compositions. Anhydrous IDPs display considerable scatter of chemical compositions at the scale of their constituents

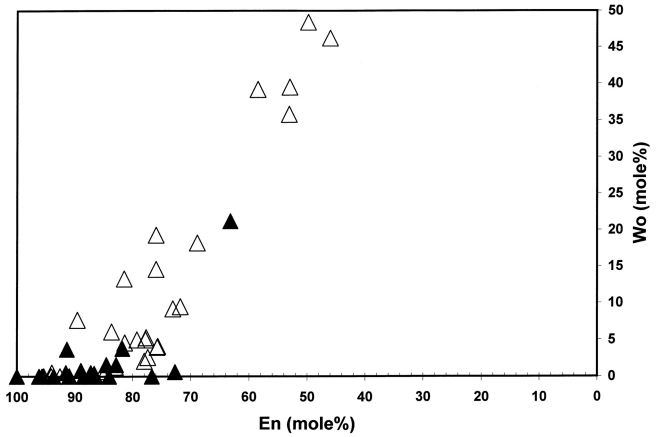

Fig. 13. Wollastonite contents as a function of enstatite (mole%) for pyroxenes in cg PCs (open triangles) and isolated pyroxenes in aggregate IDP L2011A9.

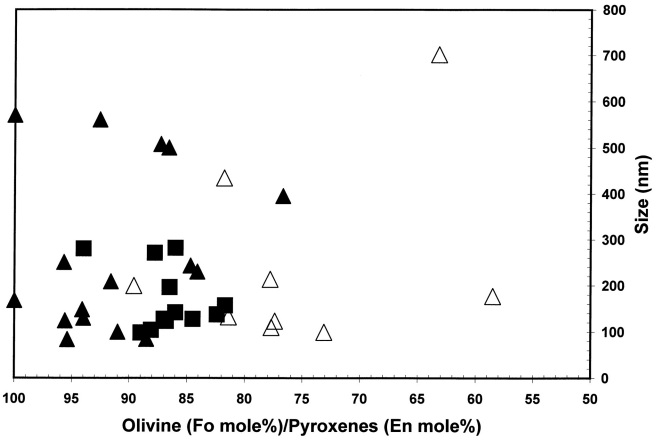

Fig. 14. Grains sizes (nm) of olivine (solid squares), pyroxenes, 0 < Wo < 2 (solid triangles), and Ca-rich pyroxenes (open triangles) in the coarse-grained PCs of aggregate IDP L2011A9.

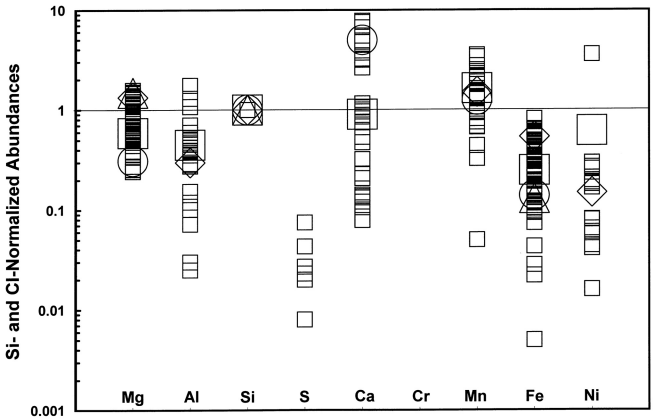

Fig. 15. Si- and CI-normalized elemental abundances for silicates in cg PCs in aggregate IDP L2011A9 (Table 4). The large symbols are the calculated average compositions of forsterite (open triangles), olivine (open diamonds), Ca-free/low-Ca pyroxene (open squares) and Ca-rich pyroxene.

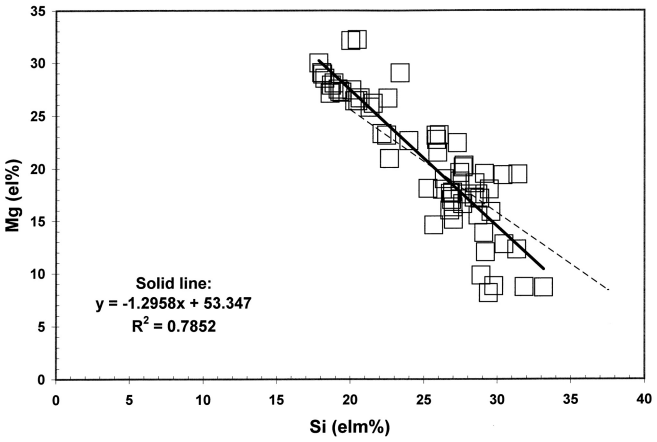

Fig. 16. Mg versus Si (el%) for silicates in coarse-grained PCs of aggregate IDP L2011A9 showing an anti-correlated linear relationship (solid line) that resembles this relationship for amorphous grains (Fig. 10) in the same cg PCs (dashed line).

(Bradley 1988). Aggregate IDP L2011A9 is no exception with its simple binary mixture of Mg,Fe-silicates and Fe,Ni-sulfides that is the common feature of the hierarchy of dust aggregation. It is also present in the Si-rich Stardust glass with the multitude of Fe-Ni-S nanograins wherein this binary hierarchical petrologic makeup was transformed and redistributed as immiscible "silicate" and "sulfide" melts and metastable Fe,Ni and S separation in chemically zoned Fe(Ni)S compounds (Zolensky et al. 2006; Leroux et al. 2008b; Rietmeijer 2007, 2008a; Rietmeijer et al. 2008). It is reasonable that some fraction of small Wild 2 loosely bonded grains or agglomerates had fused into denser agglomerates that resembled a dense agglomerate mass in IDP L2011A9 prior to interacting with the hot aerogel. The element distribution patterns of the Si-rich Stardust glass should thus resemble some combination of ufg PCs, cg PCs, Si-rich amorphous grains, Mg,Fe-silicates and Fe,Ni-sulfides, albeit now modified.

The shape of the element Fe- and CI normalized distribution pattern of dense agglomerates is remarkably similar to the Stardust glass based on average Si-rich glass composition with Fe-Ni-S inclusions from several Wild 2 tracks (Fig. 18). The systematic lower than CI composition for dense agglomerates indicates that they were more Fe-rich than the Wild 2 dust that interacted with the pure silica aerogel melt. Indeed the agglomerates had embedded sulfides, whereas only rare "FeS" grains >100 nm survived in the Stardust glass. Comparing the Fe- and CI-normalized average element abundances of ufg PCs and Si-rich Stardust glass (Fig. 18), it can be said that the differences support that nanometer-scale Wild 2 grains were not dominated by ufg PC-like grains.

Olivine and pyroxenes in cg PCs are mostly between ~100 nm and ~500 nm which is in the range of Wild 2 silicates that were assimilated by the silica melt. Adding silicates to dense agglomerates, the Fe- and CI-normalized

Table 5. Compositions (μ ± σ) (at) and range of isolated sulfides in aggregate IDP L2011A9; *N*: number of observations.

	Fe	Ni	S	N
		Ni-free sulfides		
(1)	52.2 ± 2.5; 50–55		47.8 ± 2.5; 45–50	(3)
(2)	47.8 ± 1.1; 46–50		52.2 ± 1.1; 50–44	(14)
	80		20	(1)
		Low-Ni sulfides		
(1)	50.4 ± 1.7; 48–53	1.8 ± 1.0; 0.6–4	47.8 ± 1.3; 46–50	(10)
(2)	46.6 ± 1.5; 44.5–51	1.9 ± 0.8; 0.4–4 mode: 2.4	51.5 ± 1.2; 49–54	(27)
		High-Ni sulfides		
	49.4; 47–52	13.0; 12–14	37.6; 36–38	(3)

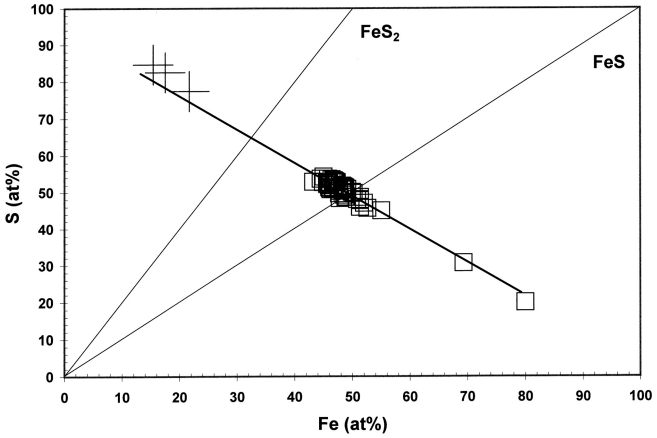

Fig. 17. Fe versus S (at%) for isolated sulfides in aggregate IDP L2011A9 (open squares) and three high-S FeS "hot spots" (crosses). Stoichiometric FeS_2 is indicated for comparison.

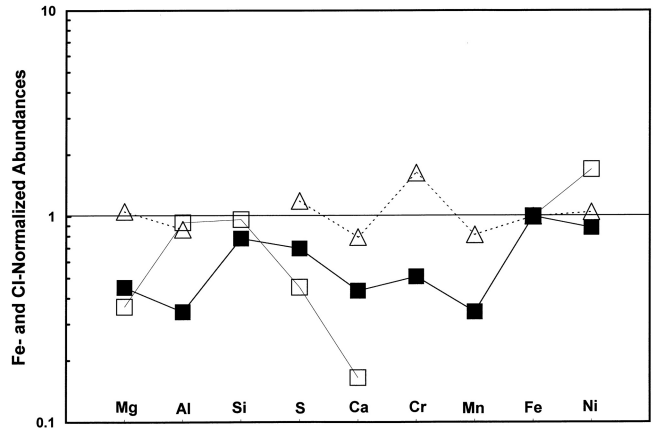

Fig. 18. Fe- and CI normalized average elemental abundances for silica-rich Stardust glass (open triangles; Leroux et al. 2008b, no silicon data; allocations FC3,0,2,2.1; C2044,2,41,3,6; C2054,0,35,51.3; C2054,1,35,44,6; C2004,1,44,4,2) compared to the dense agglomerates (solid squares) and ultrafine-grained PCs (open squares) in aggregate IDP L2011A9.

abundances would move the Mg and Ca abundances close to the a Si-rich glass composition, but it would simultaneously lower Mn and Ni abundances (Fig. 19). A mixture of dense agglomerate and amorphous materials may provide a better match with the Si-rich Stardust glass, but the IDP is higher in Ca and Mn (Fig. 19). A chemical mix of the average compositions for dense agglomerates, ufg PCs and amorphous materials is a close resemblance to Si-rich Stardust glass (Fig. 20). The very low normalized Cr abundances in the IDP L2011A9, supports the notion that a high Cr content is a unique nanometer-scale Wild 2 grain property. The Wild 2 grains resembled mixtures of these constituents found in the matrix of chondritic aggregate IDPs plus a few silicates (<500 nm) and Fe,Ni-sulfides (<100 nm).

Wild 2 and Aerogel Melt Mixing

Constituent Grain Sizes

The smallest surviving olivine (Fo_{80}) and pyroxene in the Stardust glass are 400–500 nm in size. They are apparently rare because no other studies of similar Si-rich glass from a number of different deceleration tracks reported surviving grains (Nakamura et al. 2008; Tomeoka et al. 2008; Zolensky et al. 2008). Some surviving Wild 2 silicates are comparable to the largest silicates in IDP L2011A9 (Table 6). The smaller fraction of IDP silicates would be assimilated in the Si-rich glass.

An angular surviving "FeS" grain in allocation C2004,1,44,4,3 is ~100 nm in size (Rietmeijer 2007) but there are no reports of other surviving sulfides (Nakamura et al. 2008; Tomeoka et al. 2008; Zolensky et al. 2008). Rare subhedral kamacite grains (~125 nm; ~200 nm) were present in the Si-rich glass of sample C2004-1-44-4-4; the largest grain is a single-crystal (Tomeoka et al. 2008). They could be surviving Wild 2 minerals that were slightly rounded during hypervelocity capture. Most sulfides in IDP L2011A9 are smaller than ~100 nm (Table 6) which would predict (1) an abundance of small sulfides mostly from ufg PC-like materials among Wild 2 grains to interact with the melted aerogel, and (2) a scarcity of sulfides among nanometer scale comet grains that could have survived. The grain size data support a similar makeup for the nanometer-scale Wild 2 grains that derived from the preserved

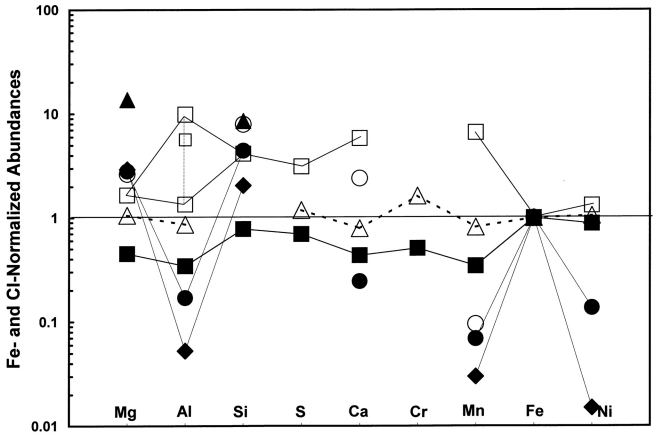

Fig. 19. Average Fe- and CI-normalized element abundances in Si-rich Stardust glass (open triangles; Leroux et al. 2008b) compared to the dense agglomerate bulk composition (solid squares), forsterite (solid triangles), Mg-rich olivine (solid diamonds), Ca-free and low-Ca pyroxene (dots) and Ca-rich pyroxene (open circles) in aggregate IDP L2011A9, and amorphous materials (open squares), including both Al populations and the average value (small open square).

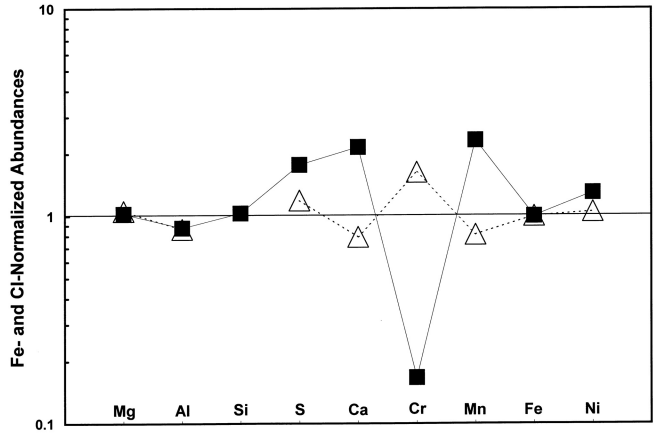

Fig. 20. Average Fe- and CI-normalized element abundances in Si-rich Stardust glass (open triangles; Leroux et al. 2008b) compared to the same element abundances in a mixture of dense agglomerates, ufg PCs and amorphous materials in aggregate IDP L2011A9 (solid squares).

chemical signature. A single cutoff size for silicate and sulfide survival seems unlikely. It should be a function of the amount of kinetic energy to be dissipated during hypervelocity impact at 6.1.km/s. A unique size cutoff would point to a similar mass (and size) of the nanometer-scale comet grains.

Wild 2 Contaminated Aerogel Melt

Comet Wild 2 showed chemical heterogeneity at the whole track level (Flynn et al. 2006) and in the Si-rich glass (Leroux et al. 2008b). The chemical properties of most common vesicular glass and the massive Si-rich Stardust glass are a binary mixture of comet materials that did not survive intact and silica from aerogel of the capture cells (Rietmeijer 2007). The glass compositions are an admixture of ~5 to ~10% of CI-like comet material and pure silica (Leroux et al. 2008b). Most primitive extraterrestrial materials are primarily simple binary mixtures of pure-Mg and Mg-rich silicates (olivine and pyroxenes) and Fe,Ni-sulfides and Fe,Ni-metals. This hierarchical or fractal pattern is seen in the matrix of aggregate IDPs (Rietmeijer 1998a) and in cluster IDPs with constituents in the 10–15 micrometer range (Rietmeijer 2002; Rietmeijer and Nuth 2004) that include chondritic aggregate IDPs and large non-chondritic particles of a wide range of chemical and mineralogical variation (Zolensky and Barrett 1992; Thomas et al. 1995; Rietmeijer 2004, 2005). There is no reason to doubt that this binary pattern was not repeated in comet Wild 2 from the nanometer scale up to the largest mineralogical diverse terminal particles.

I will assume that the silicate and Fe,Ni-sulfide and Fe,Ni-metal fractions are represented by Mg and Fe, respectively, in the Si-rich glass and the (Si- and Mg-free) Fe-Ni-S inclusions (Fig. 21). The compositions for inclusions >35 nm will plot at Si = 0, but analyses for smaller grains will be "contaminated" with the pure silica glass for Si <12el% along a mixing line (Fig. 21); for ~12 < Si (el%) <35 there is also Si from amorphous materials and silicates. The average Mg and Fe contents are for dense agglomerates and the ufg PCs in IDP L2011A9 are shown; in this diagram the Fe contents are indistinguishable. Olivine and pyroxene compositions of Wild 2 will plot on the linear correlation line for pure-Mg and Mg-rich silicates in the IDP (Fig. 21). This (dashed) line ends at Si = 37% where its extension (solid line) defines the magnesiosilica compositions of non-vesicular glass. This change from silicate to glass occurs when the magnesisilica glass has a high-silica deep metastable eutectic composition (Rietmeijer et al. 2002). Also indicated are the Mg and Fe compositions of amorphous materials in IDP L20011A9 (Fig. 21). No crystalline or amorphous silicate material has Si > 45 el%, which creates a small gap between this and the pure silica aerogel (Si = 46.75 el%) compositions.

Nanometer-Scale Wild 2 Grain Signatures

The vesicular glass data for three allocations prepared from extracted glass particles from three different Stardust deceleration tracks are presented in the Mg (el) and Fe (el) versus Si (el) diagram (Fig. 22). The allocation C2092,2,80,44,47,6 (Fig. 22a) is from a bulbous Type B track (inset) with a maximum width of ~1700 μm; the entrance hole is ~410 μm. It was located very close to the entrance hole. The data show Fe-S and Fe-metal inclusions with a wide range of "contaminant" silica glass due to decreasing inclusion sizes. That is, inclusions from >35 nm to only a few nanometers and dusty glass sprinkled with inclusions one to a few nanometers (Fig. 22a). The Ni content was not considered, which accounts for some of the scatter in the data although Ni

Table 6. Grain sizes (nanometers) of Fe-Ni-S compounds, sulfides and dust-rich patches in the Si-rich in Stardust glass (Leroux et al. 2008b; Rietmeijer et al. 2008) and in IDP L2011A9 (this study).

	<100 nm	100–200 nm	200–300 nm	300–400 nm	400–500 nm	>500 nm
			Comet 81P/Wild 2, Silica-rich Glass			
FeNiS compounds	1–~100					
"FeS"		100				
Olivine/Pyroxenes					390 × 170 to 600 × 360	
Dust-rich patches			250 × 125 to 400 × 200 (*)			~1200*
			Aggregate IDP L2011A9			
ufg PCs	30		145 ± 65	360		
Grains in ufg PCs	0.7–75					
cg PCs		135		Modal value 395	500 ± 260; 1400; Extreme: 1850 × 690	
Grains in cg PCs	8	103 ± 82.5		385	Extreme: 570 to 2050	
Sulfides#	35–(60 × 40)					
Olivine/Pyroxenes			100–500			
Isolated sulfides	38.5; modal range 95 × 70 – 125 × 90					930 × 750
Big Guy						2000 × 1000
Sulfide in matrix						1000 × 1000

*: dust-rich patches can be as small as ~300 to 450 nm or as large as 1000 nm × 625 nm to 1000 nm × 800 nm.
#: small sulfides in amorphous material of cg PCs.

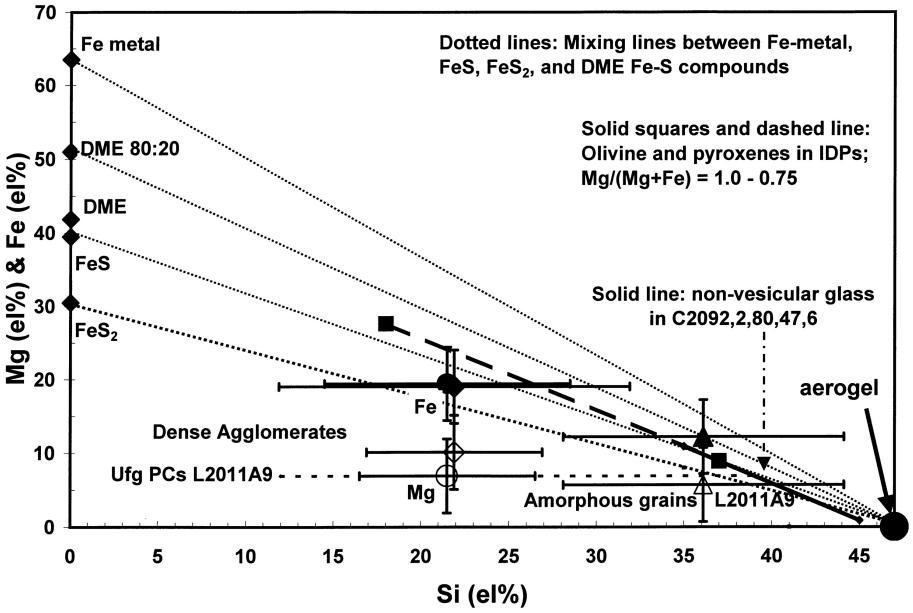

Fig. 21. A Mg (el%) and Fe (el%) versus Si (el%) diagram showing mixing lines (dotted) between Fe-S and Fe-metal grain compositions and pure silica aerogel (dot). The average Mg (open symbols) and Fe (closed symbols) contents are for dense agglomerates (diamonds), ufg PCs (circles) and amorphous grains (triangles) in chondritic aggregate IDP L20011A9. The solid lines through these symbols represent the two sigma range; the dotted line represent the full range of Si (el%) contents of ufg PCs, including GEMS and unequilibrated units (Bradley 1994a, 1994b). The dashed line between the solid squares marks olivine and pyroxene compositions in this IDP. The solid line extension represents non-vesicular magnesiosilica glass in Stardust allocation C2092,2,80,44,47,6.

contents are low. The Mg contents indicate ufg-PC and/or dense agglomerate-like materials with up to ~20 el% Fe. The fraction of Fe associated with Fe-Ni-S compounds within the appropriate Si range (Fig. 21) remains to be assessed. Glass with a uniformly low Mg content is present across the entire range of zero to Si = 45 el%. Magnesium in glass with Si <12 wt% cannot be derived from the silicates or amorphous Wild 2 materials.

Allocation C2054,0,35,44,6 was extracted from a type C bulb track(#35) with multiple styli (inset). The data show (1) abundant Fe-S and Fe-metal inclusions, (2) Ni-free Fe-S compounds with sulfur in excess of stoichiometric FeS, (3)

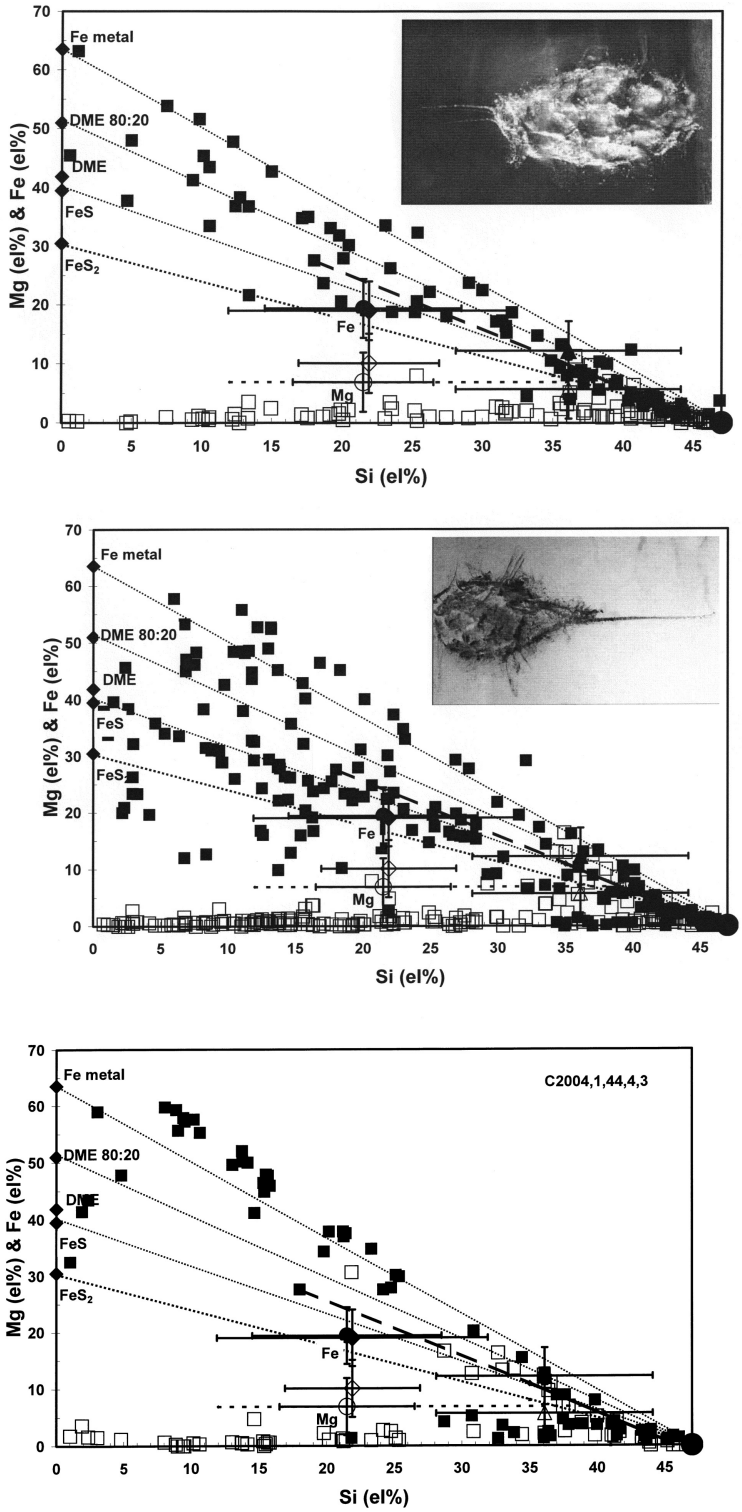

Fig. 22. The Mg and Fe (el%) versus Si (el%) diagram showing the Mg (open squares) and Fe (solid squares) contents in Si-rich glass of three allocations. a) C2092,2,80,44,47,6 from track #80 in the C2092,3,80,0,0 keystone (optical image: NASA Johnson Space Center Stardust Curatorial website). The entrance hole is at the right hand site of the image. It has three styli that measure on the order of ~4800 and 4475 μm in length. b) C2054,0,35,44,6 from track 35 that has a length/depth ratio of ~1.17 (cm) and multiple grains <40 μm (optical image: ibid.). The entrance hole is at the left hand site of the image. It has multiple styli radiating from the bulb and a single long stylus. c) C2004,1,44,4,3 was extracted from the huge track #44 that is a secondary impact feature. The comet particle first struck the aluminum collector frame, and then material from both the particle and the Al-tray together penetrated to a depth of ~0.8 cm into the aerogel (no optical image available).

ufg-PC and/or dense agglomerate-like material that could have a high (~20 el%) Fe content and (4) low-Fe magnesiosilica glass. Vesicular, low-Mg glass, 0 < Si (el%) <45 also abounds (Fig. 22b).

In this, and the previous, allocation compositions ~12 < Si (el) < 35 (el) can either indicate silica "contaminated" sulfide and metal inclusions or "contaminated" silicate material either amorphous of crystalline. It is possible to use sulfur to constrain the fractions of iron associated with the Fe-Ni-S inclusions and silicates. The Al and Ca abundances could be used to further define glass compositions Si > 35 (el) associated with amorphous materials in the IDP.

Allocation C2004,1,44,4,3 was prepared from grains taken off of a small piece of aerogel at the front of cometary track #44 of cell C2004 (Rietmeijer et al. 2008). This track, which is the largest impact feature on the cometary dust collector, was as a hedgehog type track. So far, it is the only track wherein new minerals, i.e., a number of high Si, Fe-silicide phases formed during the interactions among the Wild 2 grains and the silica melt in the reducing conditions near the front of the this track (Rietmeijer et al. 2008; Nakamura et al. 2008). The preserved compositions (Fig. 22c) show a distinct binary distribution of (1) a few Fe-S compounds, (2) many Fe-metal compounds with high-Si contents (Fe-silicides), (3) silicates, and (4) the same extended Si range for low-Mg vesicular glass. The silicate is Forsterite, $Fo_{98}Fa_2$ (Rietmeijer 2007).

To draw any conclusions with three examples would be unwise but the chemical signatures of nanometer scale Wild 2 preserved in Si-rich glass are recognizable, and using the chemical and petrologic data for chondrite aggregate IDP L2011A9 interpretable as the common materials in the matrix of aggregate IDPs.

A Chemical Background

Among others, Stephan et al. (2008) raised the possibility of a chemical background in flight aerogel perhaps inherited from the contaminants present in the preflight aerogel. The Si-rich glass with >40 Si el% is almost clear of visible electron-opaque Fe-Ni-S compound inclusions. Dusty glass that is almost free of vesicles invariably contains small amounts of Mg, Fe, S and other trace elements that could have been emplaced as fine liquid-sprays or vapors. If these elements were derived from the comet grains, vesicular glass Si <12 el% should not contain magnesium (Fig. 21). When a small fraction of comet matter was evaporated under reducing conditions during hypervelocity capture, it was perhaps possible for Mg-Fe-Ni-S vapors to penetrate the entire melt. Once precipitated, they created a pervasive chemical background in vesicular and non-vesicular glasses. Perhaps they even penetrated flight aerogel. The alternative would be that the chemical background was enhanced from ppb-level chemical impurities in pre-flight aerogel (Tsou et al. 2003). The concentration mechanism to percentage level Mg, Al, S, Ca, Cr, Mn, and Fe concentrations in flight aerogel prior to melting is currently unknown.

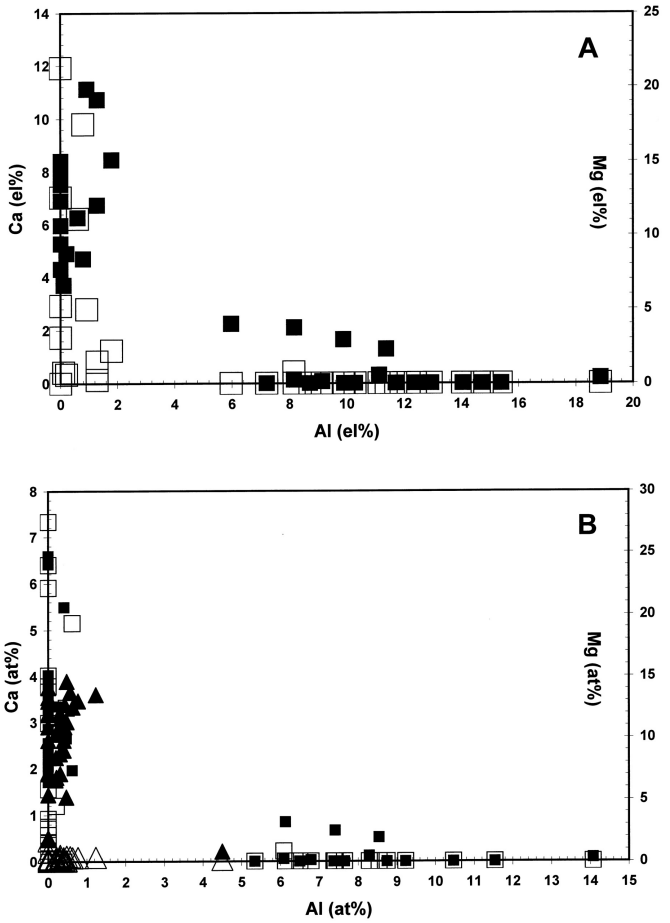

Fig. 23. a) Ca versus Al el% (open squares) and Mg versus Al el% (solid squares) in Big Guy's chemical domains in aggregate IDP L2011A9 and b) the same data for the IDP data, but expressed in atomic abundances for comparison with Al versus Ca (open triangles) and Al versus Mg (solid triangles) for "dust-rich areas" from Leroux et al. (2008b; Table 5).

Refractory glass

Amorphous Mg-rich, Mg-Al-Ca patches (Leroux et al. 2008b; Rietmeijer at al. 2008) and Si-O-Al grains (Tomeoka et al. 2008) in Si-rich glass suggest that some comet grains were refractory in nature. These discrete areas of non-vesicular glass form islands of "ghost minerals or mineral assemblages" not larger than one micrometer in the common vesicular Si-rich glass that were referred to as dust-rich patches" (Leroux et al. 2008b). The Si-rich amorphous Big Guy grain in IDP L20011A9 is of similar size and consists of chemical domains of variable Mg,Ca,Al compositions (Fig. 23a). It is more Fe-rich than the "dust-rich patches."

Al_2O_3 and CaO in silica-rich melts affect its glass-forming ability defined by a metastable miscibility gap (MacDowell and Beall 1969). For glasses in the SiO_2-Al_2O_3 system the glass-forming ability diminishes at about >10 wt% Al_2O_3, or >5.3 Al (el). There are indications for a miscibility gap in SiO_2-CaO melts whereby "high" CaO concentrations

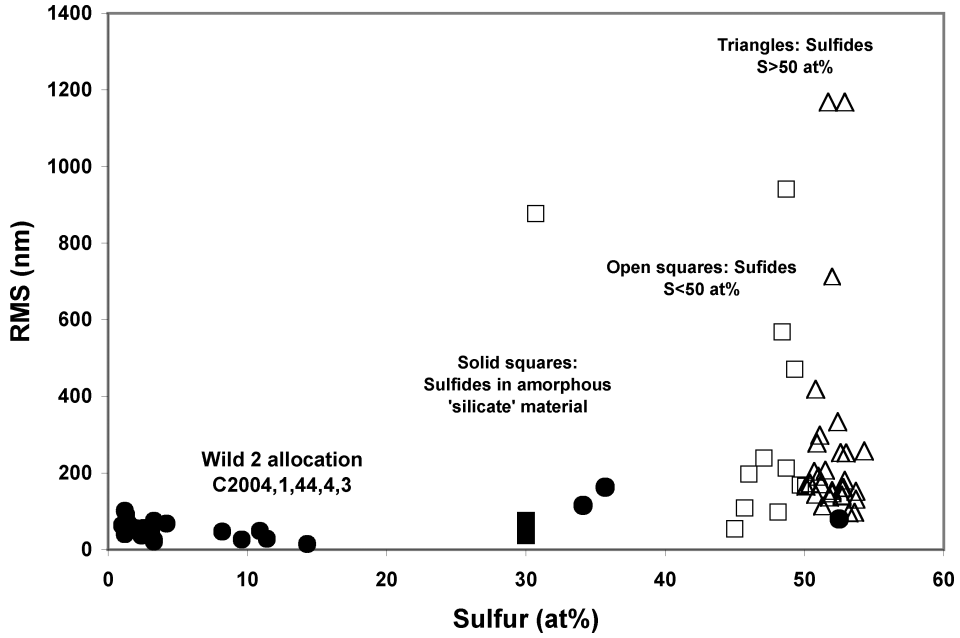

Fig. 24. Sulfur (at%) versus the root-mean-square (*rms*) sulfide grain size, >FeS (open triangles) and <FeS (open squares), of isolated sulfides, in cg PCs and Fe-Ni-S compounds in amorphous material (solid squares) in aggregate IDP L2011A9 and this relationship for a surviving "FeS" grain and spherical Fe-Ni-S inclusions in Si-rich vesicular glass of allocation C2004,1,44,4,3 (dots).The Stardust inclusion *rms* diameter would be 1.42 times larger then shown, which is insignificant at the scale of in this diagram.

would decrease the glass-forming ability (MacDowell and Beall 1969). The "dust-rich patches" reflect diminishing glass-forming abilities of Al-Si-O and Mg-Al-Ca-O melts with increasing Al and Ca concentrations generated during hypervelocity capture of Wild 2 dust in aerogel melt. They would survive as patches with deep metastable eutectic compositions (Rietmeijer and Karner 1999). Comparing the IDP and "dust-rich patches" compositions in Stardust glass (Fig. 23b) shows that most Al-Mg-O melts and a fraction of high-Ca, Ca-Mg-O would not be assimilated in Si-rich Stardust glass.

Fe-Ni-S Sulfides and Compounds

The sulfides in IDP L2011A9 are not surprisingly larger than the Fe-Ni-S compounds in vesicular Si-rich glass of allocation C2004,1,44,4,3 (Fig. 24). There is some overlap in sulfur contents between the larger Stardust grains and in the smaller grains in the IDP. These data show that nanometer-scale "FeS" grains were the most likely Wild 2 sulfides to interact with a silica melt.

The Ni-free and low-Ni Fe-S compounds entrapped in the Si-rich Stardust glass appears to define a continuous trend from Fe,Ni-metal to "FeS" (pyrrhotite) (Zolensky et al. 2006) and high sulfur hot spots between "FeS" and sulfur (Leroux et al. 2008b). The Ni-free and low-Ni Fe-S compound compositions show discrete groupings of preferred compositions in Stardust glass and in IDP L2011A9 (Table 7), except for the core compositions of chemically zoned Fe-Ni-S compounds in Stardust glass. The Fe-S phase diagram (Rietmeijer et al. 2008) shows how the compounds listed in Table 7 can have one of three deep metastable eutectic compositions at (1) almost stoichiometric FeS, (2) S ≈ 10 (el) and (3) S ≈ 20 (el) (Rietmeijer 2008). These unique compositions and the high-S compounds suggest the decomposition of "FeS" melt into low- and high-sulfur melts at temperatures >1200 °C and reducing conditions for the modified Wild 2 grains and in IDP L2011A9. Many of the larger Fe-Ni-S compound grains have a core-mantle structure. The shape of some of these mantles (cf. Leroux et al. 2008b) suggests they moved through a "viscous" of still liquid silica melt (Rietmeijer 2008). The absence of core-mantle structures for the Fe-Ni-S compounds in aggregate IDP L2011A9, and in fact in all aggregate IDPs (Rietmeijer 1998a) points to much less dynamic environments during thermal modification in aggregate IDP parent bodies compared to the conditions during hypervelocity capture of the nanometer-scale Wild 2 grains (Ishii et al. 2008).

Table 7. Average sulfur (el%) contents of Ni-free and low-Ni Fe-S compounds in aggregate IDP L2011A9 and electron opaque inclusions in Si-rich vesicular Stardust glass (Rietmeijer 2008a).

IDP L2011A9		Wild 2
38.5		38 (fragment)
34.5		33 ± 3 (rim)
20	[21]	
		9 ± 2 (core)

CONCLUSIONS

The observation that chondritic aggregate IDPs and therefore also cluster IDPs do not originate in the same parent bodies that provided meteorites implies that searching for the parent bodies of comet dust should first turn to these IDPs. The combination of composition (Jessberger et al. 1988) and mass (size) (Fomenkova et al. 1992) suggest that the nanometer-scale comet Halley dust resembled the properties of ufg PCs and cg PCs in IDPs (Rietmeijer 2002). The silica aerogel properties favored intact survival of micrometer-scale grains Wild 2 at the expense of the numerous nanometer-scale grains that have yet to be found. They were completely melted and modified during hypervelocity capture, but they left their chemical signatures in the typically vesicular Si-rich glass with the characteristic numerous Fe-Ni-S compound inclusions.

Using the petrologic, mineralogical and chemical properties of the constituents in chondritic aggregate IDP L2011A9, which is typical of aggregate IDPs that experienced pre-entry thermal modification, it was possible to interpret the comet's chemical signatures in allocations from three different Stardust deceleration tracks.

The nanometer-scale Wild 2 grains resembled variable mixtures of ufg-PC and/or dense agglomerate-like material, Mg-rich silicates (<500 nm) and Fe,Ni-sulfides (<100 nm). The still small sample also suggests the presence of amorphous Si-rich materials and Fe,Ni-metal in Wild 2 grains. These chemical signatures also have more subtle information on Fe partitioning between silicates and Fe-Ni-S compounds, Mg/(Mg + Fe) ratios, Fe-Ni-S compound compositions. The main conclusion is that comets Halley and Wild 2 contain nanometer scale grains with the chemical, and therefore also petrologic, properties of the constituents that are found in the matrix of the most common chondritic aggregate IDPs. The nanometer-scale particles were pervasive in the accretion zones of both Halley type and J-F type comets. More work is needed to search for systematic trends or significant differences in the makeup of the Wild 2 nanometer scale grains from their chemical signatures in Si-rich glass.

Acknowledgments—I thank an anonymous reviewer and the handling editor for constructive comments. This work was supported by NASA grant NNX07AM65G through the NASA Stardust Analyses Program. The analyses were conducted in the Electron Microbeam Analyses Facility in the Department of Earth and Planetary Sciences at UNM.

Editorial Handling—Dr. Scott Sandford

REFERENCES

A'Hearn M. F., Belton M. J. S., Delamere W. A., Kissel J., Klaasen K. P., McFadden L. A., Meech K. J., Melosh H. J., Schultz P. H., Sunshine J. M., Thomas P. C., Veverka J., Yeomans D. K., Baca M. W., Busko I., Crockett C. J., Collins S. M., Desnoyer M., Eberhardy C. A., Ernst C. M., Farnham T. L., Feaga L., Groussin O., Hampton D., Ipatov S. I., Li J.-Y., Lindler D., Lisse C. M., Mastrodemos N., Owen Jr. W. M., Richardson J. E., Wellnitz D. D., and White R. L. 2005. Deep Impact: Excavating comet Tempel 1. *Science* 310:258–264.

Anders E. and Grevesse N. 1989. Abundances of the elements: Meteoritic and solar. *Geochimica et Cosmochimica Acta* 53:197–214.

Borovička J. 2005. Elemental abundances in Leonid and Perseid meteoroids. In *Modern meteor science, An interdisciplinary view*, edited by R. Hawkes, I. Mann, and P. Brown. Berlin: Springer-Verlag. pp. 245–253.

Borovička J. 2006. Physical and chemical properties of meteoroids as deduced from observations. In *Asteroids, Comets, Meteors 2005, Proceedings of the IAU Symposium 229*, edited by Lazzaro D., Ferraz-Mello S., and Fernandez J. A. pp. 249–271.

Borovička J., Koten P. Spurný P. Boček J., and Štork R. 2005. A survey of meteor spectra and orbits: Evidence for three populations of Na-free meteoroids. *Icarus* 174:15–30.

Bradley J. P. 1988. Analysis of chondritic interplanetary dust thin-sections. *Geochimica et Cosmochimica Acta* 52:889–900.

Bradley J. P. 1994a. Chemically anomalous, pre-accretionally irradiated grains in interplanetary dust from comets. *Science* 265: 925–929.

Bradley J. P. 1994b. Nanometer-scale mineralogy and petrography of fine-grained aggregates in anhydrous interplanetary dust particles. *Geochimica et Cosmochimica Acta* 58:2123–2134.

Bradley J. P. and Brownlee D. E. 1986. Cometary particles: Thin sectioning and electron beam analysis. *Science* 231:1542–1544.

Bradley J. P. and Ishii H. A. 2008. Comment on "The shape and composition of interstellar silicate grains." *Astronomy & Astrophysics* 486:781–784.

Brown M. E., Barkume K. M., Ragozzine D., and Schaller E. L. 2007. A collisional family of icy objects in the Kuiper belt. *Nature* 466: 294–296.

Brownlee D. E., Hörz F., Newburn R. L., Zolensky M., Duxbury T. C., Sandford S., Sekanina Z., Tsou P., Hanner M. S., Clark B. C., Green S. F., and Kissel J. 2004. Surface of young Jupiter-family comet 81P/Wild 2: View from the Stardust spacecraft. *Science* 304:1764–1769.

Brownlee D., Tsou P., Aléon J., Alexander, C. M. O'D., Araki T., Bajt S., Baratta G. A., Bastien R., Bland Ph., Bleuet P., Borg J., Bradley J. P., Brearley A., Brenker F., Brennan S., Bridges J. C., Browning N. D., Brucato J. R., Bullock E., Burchell M. J., Busemann H., Butterworth A., Chaussidon M., Cheuvront A., Chi M., Cintala M. J., Clark B. C., Clemett S. J., Cody G., Colangeli L., Cooper G., Cordier P., Daghlian C., Dai Z., D'Hendecourt L., Djouadi Z., Dominguez G., Duxbury T., Dworkin J. P., Ebel D. S., Economou T. E., Fakra S., Fairey S. A. J., Fallon S., Ferrini G., Ferroir T., Fleckenstein H., Floss C., Flynn G., Franchi I. A., Fries M., Gainsforth Z., Gallien J.-P., Genge M., Gilles M. K., Gillet P., Gilmour J., Glavin D. P., Gounelle M., Grady M. M., Graham G. A., Grant P. G., Green S. F., Grossemy F., Grossman L., Grossman J. N., Guan Y., Hagiya H., Harvey R., Heck P., Herzog G. F., Hoppe P., Hörz F., Huth J., Hutcheon I. D., Ignatyev K., Ishii H., Ito M., Jacob D., Jacobsen C., Jacobsen S., Jones S., Joswiak D., Jurewicz A., Kearsley A. T., Keller L. P., Khodja H., Kilcoyne A. L. D., Kissel J., Krot A., Langenhorst F., Lanzirotti A., Le L., Leshin L. A., Leitner J., Lemelle L., Leroux H., Liu M-C., Luening K., Lyon I., MacPherson G., Marcus M. A., Marhas K., Marty B., Matrajt G., McKeegan K., Meibom A., Mennella V., Messenger K., Messenger S., Mikouchi T., Mostefaoui S., Nakamura T., Nakano

T., Newville M., Nittler L. R., Ohnishi I., Ohsumi K., Okudaira K., Papanastassiou D. A., Palma R., Palumbo M. E., Pepin R. O., Perkins D., Perronnet M., Pianetta P., Rao W., Rietmeijer F. J. M., Robert F., Rost D., Rotundi A., Ryan R., Sandford S. A., Schwandt G. S., See T. H., Schlutter D., Sheffield-Parker J., Simionovici A., Simon S., Sitnitsky I., Snead C. J., Spencer M. K., Stadermann F., Steele A., Stephan T., Stroud R., Susini J., Sutton S. R., Suzuki Y., Taheri M., Taylor S., Teslich N., Tomeoka K., Tomioka N., Toppani A., Trigo-Rodríguez J. M., Troadec D., Tsuchiyama A., Tuzzolino A. J., Tyliszczak T., Uesugi K., Velbel M., Vellenga J., Vicenzi E., Vincze L., Warren J., Weber I., Weisberg M., Westphal A. J., Wirick S., Wooden D., Wopenka B., Wozniakiewicz P., Wright I., Yabuta H., Yano H., Young E. D., Zare R. N., Zega T., Ziegler K., Zimmerman L., Zinner E., and Zolensky M. 2006. Comet 81P/Wild 2 under a microscope. *Science* 314:1711–1716.

Cliff G. and Lorimer G. W. 1975. The quantitative analysis of thin specimens. *Journal of Microscopy* 103:203–207.

Dai Z. R. and Bradley J. P. 2001. Iron-nickel sulfides in anhydrous interplanetary dust particles. *Geochimica et Cosmochimica Acta* 65:3601–3612.

Flynn G. J. 1994a. Interplanetary dust particles collected from the stratosphere: Physical, chemical and mineralogical properties and implications for their sources. *Planetary and Space Science* 42:1151–1161.

Flynn G. J. 1994b. The common stuff of stardust. *Nature* 371:287–288.

Flynn G. J., Bleuet P, Borg J., Bradley J. P., Brenker F. E., Brennan S., Bridges J., Brownlee D. E., Bullock E. S., Burghamme M., Clark B. C., Dai Z. R., Daghlian C. P., Djouadi Z., Fakra S., Ferroir T., Floss C., Franchi I. A., Gainsforth Z., Gallien J. P., Gillet Ph., Grant P. G., Graham G. A., Green S. F., Grossemy F., Heck P. R., Herzog G. F., Hoppe P., Hörz F., Huth J., Ignatyev K., Ishii H. A., Janssens K., Joswiak D., Kearsley A. T., Khodja H., Lanzirotti A., Leitner J., Lemelle L., Leroux H., Luening K., MacPherson G. J., Marhas K. K., Marcus M. A., Matrajt G., Nakamura T., Nakamura-Messenger K., Nakano T., Newville M., Papanastassiou D. A., Pianetta P., Rao W., Riekel C., Rietmeijer F. J. M., Rost D., Schwandt G. S., See T. H., Sheffield-Parker J., Simionovici A., Sitnitsky I., Snead C. J., Stadermann F. J., Stephan T., Stroud R. M., Susini J., Suzuki Y., Sutton S. R., Taylor S., Teslich N., Troadec D., Tsou P., Tsuchiyama A., Uesugi K., Vekemans B., Vicenzi E. P, Vincze L., Westphal A. J., Wozniakiewicz P., Zinner E., and Zolensky M. E. 2006. Elemental compositions of comet 81P/Wild 2 samples collected by Stardust. *Science* 314:1731–1735.

Fomenkova M. N., Kerridge J. F., Marti K., and McFadden L.-A. 1992. Compositional trends in rock-forming elements of comet Halley dust. *Science* 258:266–269.

Ishii H. A., Bradley J. P., Dai Z. R., Chi M., Kearsley A. T., Burchell M. J., Browning N. D., and Molster F. 2008. Comparison of comet 81P/Wild 2 dust with interplanetary dust from comets. *Science* 319:447–450.

Jenniskens P. 2006. *Meteor showers and their parent comets*. Cambridge: Cambridge University Press. 790 p.

Jessberger E. K., Christoforidis A., and Kissel J. 1988. Aspects of major element composition of Halley's dust. *Nature* 332:691–695.

Joswiak D J. and Brownlee D. E. 1998. Atmospheric entry melting in 5–15 μm hydrous IDPS: Evidence from analytical TEM studies and pulse-heating experiments (abstract #1929). 29th Lunar and Planetary Science Conference. CD-ROM.

Joswiak D. J. and Brownlee D. E. 2006. Non-GEMS silicate glasses in chondritic porous interplanetary dust particles (abstract #2190). 37th Lunar and Planetary Science Conference. CD-ROM.

Keller L.P. and Messenger S. 2004. On the origin of GEMS (abstract #1985). 35th LPS Lunar and Planetary Science Conference. CD-ROM.

Leroux H., Jacob D., Stodolna J., Nakamura-Messenger K., and Zolensky M. E. 2008a. Igneous Ca-rich pyroxene in comet 81P/Wild 2. *American Mineralogist* 93:1933–1936.

Leroux H., Rietmeijer F. J. M., Velbel M. A., Brearley A. J., Jacob D., Langenhorst F., Bridges J. C., Zega T. J., Stroud R. M., Cordier P., Harvey R. P., Lee M., Gounelle M., and Zolensky M. E. 2008b. A TEM study of thermally modified comet 81P/Wild 2 dust particles by interactions with the aerogel matrix during the Stardust capture process. *Meteoritics & Planetary Science* 43:97–120.

Leroux H., Rietmeijer F. J. M., Jacob D., and Roskosz M. 2008c. Evidence for hot chemistry under reduced conditions in the thermally modified STARDUST samples (abstract #1292). 39th Lunar and Planetary Science Conference. CD-ROM.

Leroux H., Roskosz M., and Jacob D. 2009. Oxidation state of iron and extensive redistribution of sulfur in thermally modified Stardust particles. *Geochimica et Cosmochimica Acta* 73:767–777.

Lindsley D. H. and Andersen D. J. 1983. A two-pyroxene thermometer. Proceedings, 13th Lunar and Planetary Science Conference, Part 2. *Journal of Geophysical Research* 88:A887–A906.

Lyytinen E. J. and van Flandern T. 2000. Predicting the strength of Leonid outbursts. In *Leonid storm research*, edited by Jenniskens P., Rietmeijer F. J. M., Brosch N., and Fonda M. Dordrecht, The Netherlands: Kluwer Academic Publishers. pp. 149–166,

MacDowell J. F. and Beall G. H. 1969. Immiscibility and crystallization in Al_2O_3–SiO_2 glasses. *Journal of the American Ceramic Society* 52:17–25.

Mackinnon I. D. R. and Rietmeijer F. J. M. 1987. Mineralogy of chondritic interplanetary dust particles. *Reviews in Geophysics* 25:1527–1553.

McNaught R. H. and Asher D. J. 1999 Leonid dust trails and meteor storms. *WGN, Journal of the International Meteor Organization* 27:85–102.

Matrajt G., Ito M., Wirick S., Messenger S., Brownlee D. E., Joswiak D., Flynn G., Sandford S., Snead C., and Westphal A. 2008 Carbon investigation of two Stardust particles: A TEM, NanoSIMS, and XANES study. *Meteoritics & Planetary Science* 43:315–334.

Martin P. G. 1995. On the value of GEMS (glass with embedded metal and sulphides). *The Astrophysical Journal* 445:L63–L66.

Min M., Waters L. B. F. M., de Koter A., Hovenier J. W., Keller L. P., and Markwick-Kemper F. 2007. The shape and composition of interstellar silicate grains. *Astronomy & Astrophysics* 462:667–676.

Nakamura T, Tsuchiyama A., Akaki T., Uesugi K., Nakano T., Takeuchi A., Suzuki Y., and Noguchi T. 2008 Bulk mineralogy and three-dimensional structures of individual Stardust particles deduced from synchrotron X-ray diffraction and microtomography analysis. *Meteoritics & Planetary Science* 43: 247–259.

Nozaki W., Nakamura T., Noguchi T., and Takaoka N. 2001. Synchrotron X-ray diffraction analysis of pulse-heated Tagish Lake carbonaceous chondrite: Experimental reproduction of micrometeorites. *KEK Progress Report* 2001-2:186.

Rietmeijer F. J. M. 1994a. A proposal for a petrological classification scheme of carbonaceous chondritic micrometeorites. In *Analysis of interplanetary dust*, edited by Zolensky M. E., Wilson T. L, Rietmeijer F. J. M., and Flynn G. J. American Institute of Physics Conference Proceedings, vol. 310. Woodbury, N.Y.: The American Institute of Physics. pp. 231–240.

Rietmeijer F. J. M. 1994b. Searching for a principal component

mixing model for chondritic interplanetary dust particles: The use of size analysis (abstract). 25th Lunar and Planetary Science Conference. pp. 1129–1130.

Rietmeijer F. J. M. 1996a. The ultrafine mineralogy of a molten interplanetary dust particle as an example of the quench regime of atmospheric entry heating. *Meteoritics & Planetary Science* 31:237–242.

Rietmeijer F. J. M. 1996b. The butterflies of principal components: A case of ultrafine-grained polyphase units (abstract). 27th Lunar and Planetary Science Conference. pp. 1073–1074.

Rietmeijer F. J. M. 1996c. A test of isochemical behavior of principal components in chondritic porous IDPs (abstract). *Meteoritics and Planetary Science* 31:A114.

Rietmeijer F. J. M. 1996d. CM-like interplanetary dust particles in the lower stratosphere during 1989 October and 1991 June/July. *Meteoritics & Planetary Science* 31:278–288.

Rietmeijer F. J. M. 1998a. Interplanetary dust particles. In *Planetary materials*, edited by Papike J. J. Reviews In Mineralogy, vol. 36. Chantilly, Virginia: Mineralogical Society of America. pp. 2-1–2-95.

Rietmeijer F. J. M. 1998b. Interplanetary dust. In *Advances in mineralogy*, vol. 3, edited by A. S. Marfunin. Berlin: Springer-Verlag. pp. 22–28.

Rietmeijer F. J. M. 1999a Metastable non-stoichiometric diopside and Mg-wollastonite: An occurrence in an interplanetary dust particle. *American Mineralogist* 84:1883–1894.

Rietmeijer F. J. M. 1999b Sodium tails of comets: Na/O and Na/Si abundances in interplanetary dust particles. *The Astrophysical Journal* 514:L125–L127.

Rietmeijer F. J. M. 1999c. Evolution of condensed pre-solar dust with metastable eutectic smectite dehydroxylate compositions: Truly GEMS (abstract #1060). 30th Lunar and Planetary Science Conference. CD-ROM.

Rietmeijer F. J. M. 2000. Interrelationships among meteoric metals, meteors, interplanetary dust, micrometeorites, and meteorites. *Meteoritics & Planetary Science* 35:1025–1041.

Rietmeijer F. J. M. 2002. The earliest chemical dust evolution in the solar nebula. *Chemie der Erde* 62:1–45.

Rietmeijer F. J. M. 2004. Dynamic pyrometamorphism during atmospheric entry of large (~10 micron) pyrrhotite fragments from cluster IDPs. *Meteoritics & Planetary Science* 39:1869–1887.

Rietmeijer F. J. M. 2005. Interplanetary dust and carbonaceous meteorites: Constraints on porosity, mineralogy and chemistry of meteors from rubble-pile planetesimals. In *Modern meteor science, An interdisciplinary view*, edited by R. Hawkes, I. Mann, and P. Brown. Berlin: Springer-Verlag. pp. 321–338.

Rietmeijer F. J. M. 2007. Challenges to understand aerogel contaminated by hypervelocity-impacted comet Wild 2 dust (abstract #1082). 38th Lunar and Planetary Science Conference. CD-ROM.

Rietmeijer F. J. M. 2008. Time, temperatures, and pressure indicated by metastable iron-sulfide nanophases in melted STARDUST aerogel (abstract #1188). 39th Lunar and Planetary Science Conference. CD-ROM.

Rietmeijer F. J. M. and Karner J. M. 1999. Metastable eutectics in the Al_2O_3–SiO_2 system explored by vapor phase condensation. *Journal of Chemical Physics* 110:4554–4558.

Rietmeijer F. J. M. and Nuth III J. A. 2000. Collected extraterrestrial materials: Constraints on meteor and fireball compositions. *Earth, Moon, and Planets* 82/83:325–350.

Rietmeijer F. J. M. and Nuth III J. A. 2002. Experimental astromineralogy: Circumstellar ferromagnesiosilica dust in analogs and natural samples. In *Dust in the solar system and other planetary systems*, edited by Green S., Williams F. I. P., McDonnell J. A. M., and McBride N. COSPAR Colloquia Series, vol. 15. Oxford: Pergamon/Elsevier. pp. 333–339.

Rietmeijer F. J. M. and Nuth III J. A. 2004. Grain sizes of ejected comet dust: Condensed dust analogs, interplanetary dust particles and meteors. In *The New ROSETTA Targets—Observation, simulations and instrument performances*, edited by L. Colangeli, E. Mazzotta Epifani, and P. Palumbo. Astrophysics Space Science Library, vol. 97–110. Kluwer Academic Publishers.

Rietmeijer F. J. M., Nuth III J. A., and Karner J. M. 1999a. Metastable eutectic condensation in a Mg-Fe-SiO-H_2-O_2 vapor: Analogs to circumstellar dust. *The Astrophysical Journal* 527:395–404.

Rietmeijer F. J. M., Nuth III J. A., and Karner J. M. 1999b. Metastable eutectic gas to solid condensation in the FeO-Fe_2O_3-SiO_2 system. *Physical Chemistry Chemical Physics* 1:1511–1516.

Rietmeijer F. J. M., Nuth III J. A., Karner J. M., and Hallenbeck S. L. 2002. Gas to solid condensation in a Mg-SiO-H_2-O_2 vapor: Metastable eutectics in the MgO–SiO_2 phase diagram. *Physical Chemistry Chemical Physics* 4:546–551.

Rietmeijer F. J. M., Nuth III J. A., Rochette P., Marfaing J., Pun A., and Karner J. M. 2006. Deep metastable eutectic condensation in Al-Fe-SiO-O_2-H_2 vapors: Implications for natural Fe-aluminosilicates. *American Mineralogist* 91:1688–1698.

Rietmeijer F. J. M., Nakamura T., Tsuchiyama A., Uesugi K, Nakano T., and Leroux H. 2008 Origin and formation of iron-silicide phases in the aerogel of the Stardust mission. *Meteoritics & Planetary Science* 43:121–134.

Roskosz M., Watson H. C., and Leroux H. 2008a. What was the thermal history of cometary dust particles during their collect by the NASA's Stardust spacecraft? (abstract #1580). 39th Lunar and Planetary Science Conference. CD-ROM.

Roskosz M., Watson H. C., and Leroux H. 2008b. Thermal history, partial preservation and sampling bias recorded by Stardust cometary grains during their capture. *Earth and Planetary Science Letters* 273:195–202.

Soderblom L. A., Becker T. L., Bennett G., Boice D. C., Britt D. T., Brown R. H., Buratti B. J., Isbell C., Giese B., Hare T., Hicks M. D., Howington-Kraus E., Kirk R. L., Lee M., Nelson R. M., Oberst J., Owen T. C., Rayman M. D., Sandel B. R., Stern S. A., Thomas N., and Yelle R. V. 2002. Observations of comet 19P/Borrelly by the Miniature Integrated Camera and Spectrometer aboard Deep Space 1. *Science* 296:1087–1091.

Stephan T., Rost D., Vicenzi E. P., Bullock E. S., MacPherson G. J., Westphal A. J., Snead C. J., Flynn G. J., Sandford S. A., and Zolensky M. E. 2008. TOF-SIMS analysis of cometary matter in Stardust aerogel tracks. *Meteoritics & Planetary Science* 43: 233–246.

Thomas K. L., Blanford G. E., Clemett S. J., Flynn G. J., Keller L. P., Klöck W., Maechling C. R., McKay D. S., Messenger S., Nier A. O., Schlutter D. J., Sutton S. R., Warren J. L., and Zare R. N. 1995. An asteroidal breccia: The anatomy of a cluster IDP. *Geochimica et Cosmochimica Acta* 59:2797–2815.

Tomeoka K., Tomioka N., and Ohnishi I. 2008 Silicate minerals and Si-O glass in comet Wild 2 samples: Transmission electron microscopy. *Meteoritics & Planetary Science* 43:273–284.

Tsou P., Brownlee D. E., Hörz F., Sandford S. A., and Zolensky M. E. 2003. Wild 2 and interstellar sample collection and Earth return. *Journal of Geophysical Research* 108(E10): 8113, doi: 10.1029/2003JE002109.

Zolensky M. and Barrett R. 1992. Compositional variations of olivines and pyroxenes in chondritic interplanetary dust particles. *Meteoritics* 29:616–620.

Zolensky M. E., Zega T. J., Yano H., Wirick S., Westphal A. J., Weisberg M. K., Weber I., Warren J. L., Velbel M. A., Tsuchiyama A., Tsou P., Toppani A., Tomioka N., Tomeoka K., Teslich N., Taheri M., Susini J., Stroud R., Stephan T., Stadermann F. J., Snead C. J., Simon S. B., Simionovici A., See

T. J., Robert R., Rietmeijer F. J. M., Rao W., Perronnet M. C., Papanastassiou D. A., Okudaira K., Ohsumi K., Ohnishi I., Nakamura-Messenger K., Nakamura T., Mostefaoui S., Mikouchi T., Meibom A., Matrajt G., Marcus M. A., Leroux H., Lemelle L., Le L., Lanzirotti A., Langenhorst F., Krot A. N., Keller L. P, Kearsley A. T., Joswiak D., Jacob D., Ishii H., Harvey R., Hagiya K., Grossman L., Grossman J. N., Graham G. A., Gounelle M., Gillet P., Genge M. J., Flynn G., Ferroir T., Fallon S., Ebel D. S., Dai Z., Cordier P., Clark B., Chi M., Butterworth A. L., Brownlee D. E., Bridges J. C., Brennan S., Brearley A., Bradley J. P., Bleuet P., Bland P. A., and Bastien R. 2006. Mineralogy and petrology of comet Wild 2 nucleus samples. *Science* 314:1735–1739.

Zolensky M., Nakamura-Messenger K., Sverdrup J., Rietmeijer F., Leroux H., Mikouchi T., Ohsumi K., Simon S., Grossman L., Stephan T., Weisberg M., Velbel M., Zega T., Stroud R., Tomeoka K., Ohnishi, I., Tomioka N., Nakamura T., Matrajt G., Joswiak J., Brownlee D., Langenhorst F., Krot A., Kearsley A., Ishii H., Graham G., Dai Z.R., Chi M., Bradley J., Hagiya K., Gounelle M., and Bridges J. 2008. Comparing Wild 2 particles to chondrites and IDPs. *Meteoritics & Planetary Science* 43:261–272.